# Nature of the Cuvier Abyssal Plain crust, offshore NW Australia

Running title: Origin of the Cuvier Abyssal Plain

Matthew T. Reeve[1], Craig Magee[1,2]*, Ian D. Bastow[1], Carl McDermott[1], Christopher A.-L. Jackson[1,4], Rebecca E. Bell[1], Julie Prytulak[3]

[1]Basins Research Group (BRG), Department of Earth Science and Engineering, Royal School of Mines, Prince Consort Road, Imperial College London, SW7 2BP, England, UK.

[2]School of Earth and Environment, University of Leeds, Leeds, LS2 9JT, UK.

[3]Department of Earth Sciences, University of Durham, DH1 3LE, UK

[4]Department of Earth and Environmental Sciences, The University of Manchester, Williamson Building, Oxford Road, Manchester, M13 9PL, UK

*Correspondence (c.magee@leeds.ac.uk)

**Abstract**

Magnetic stripes have long been assumed to be indicative of oceanic crust. However, continental crust heavily intruded by magma can also record magnetic stripes. We re-evaluate the nature of the Cuvier Abyssal Plain (CAP), offshore NW Australia, which hosts magnetic stripes and has previously been defined as oceanic crust. We show chemical data from a basalt within the CAP, previously described as an enriched MORB, could equally be interpreted to contain evidence of contamination by continental material. We also recognise seaward-dipping reflector (SDR) sequences in seismic reflection data across the CAP. Borehole data from overlying sedimentary rocks suggests these SDRs were emplaced in a

shallow-water (<200 m depths) or sub-aerial environment. Our results indicate the CAP may not be unambiguous oceanic crust, but may instead comprise a spectrum of heavily intruded continental crust through to fully oceanic crust. If the CAP represents such a continent-ocean transition zone, adjacent unambiguous oceanic crust would be located >500 km further offshore NW Australia than currently thought; this would impact plate tectonic reconstructions, as well as heat flow and basin modelling studies. Our work also supports the growing consensus that magnetic stripes cannot, by themselves, be used to determine crustal affinity.

Supplementary material: Enlarged and uninterpreted versions of the magnetic data and seismic reflection lines are available at.

The discovery of magnetic reversal anomalies (stripes) across oceanic basins was fundamental to the development of plate tectonic theory (e.g., Vine & Matthews 1963). These magnetic anomalies arise from the interaction between the present-day magnetic field and remanent magnetizations, records of past magnetic field polarity, acquired by igneous rocks during their emplacement and crystallisation at contemporaneous seafloor spreading ridges (Tivey et al. 1998). Where magnetic stripes occur adjacent to passive continental margins, they are thus commonly interpreted to mark a basin's oldest, unambiguous oceanic crust (e.g., Talwani & Eldholm 1973; Rabinowitz & LaBrecque 1979; Veevers 1986). However, the progressive intrusion of magma into continental crust during break-up often leads to the development of broad, complex zones whose structural and geochemical character can display both a continental and oceanic affinity (e.g., Skogseid et al. 1992; Symonds et al. 1998; Planke et al. 2000; Skogseid et al. 2000; Direen et al. 2007; Bastow & Keir 2011). Linear magnetic stripes akin to those hosted by unambiguous oceanic crust have been

identified within COTZs such as: (i) the onshore Red Sea Rift in Afar, Ethiopia where continental crust is heavily intruded (Bridges et al. 2012); (ii) along the magma-poor passive margins offshore Iberia and Newfoundland, where magnetic anomalies are recorded by magmatic intrusions emplaced into exhumed and serpentinised mantle prior to break-up (Bronner et al. 2011); (iii) across part of the magma-rich passive margin offshore NW Australia (i.e. the Gascoyne margin; Direen et al. 2008); and (iv) offshore South America where the margin comprises so-called 'magmatic crust' wholly consisting of new igneous material, which differs from normal oceanic crust in that it formed via extension in a sub-aerial and/or shallow-water setting, and not true deep-marine spreading (Collier et al. 2017; McDermott et al. 2018).

Given recent studies have shown magnetic stripes may not be diagnostic of oceanic crust (e.g., Direen et al. 2008; Bridges et al. 2012; Collier et al. 2017; McDermott et al. 2018), it is worth re-evaluating the nature of areas previously defined as oceanic crust adjacent to passive margins (Eagles et al. 2015; Causer et al. 2020). For example, the Cuvier Abyssal Plain (CAP), offshore NW Australia hosts well-developed magnetic stripes distributed about inferred spreading centres and has been interpreted as unambiguous oceanic crust that formed at a half-spreading rate of ~3.5–4.5 cm $yr^{-1}$ (Fig. 1) (e.g., Falvey & Veevers 1974; Larson et al. 1979; Robb et al. 2005; Gibbons et al. 2012; MacLeod et al. 2017). Here, we investigate the origin of the CAP, offshore NW Australia through an integrated analysis of 2D seismic reflection data, magnetic data, and a re-examination of published chemical data. We show packages of seaward-dipping reflector (SDR) sequences occur across the CAP, occasionally spanning several magnetic stripes, and probably represent lavas emplaced in sub-aerial or shallow-water conditions. We reinterpret chemical data from a basalt dredged from an inferred spreading centre (the Sonne Ridge: Fig. 1A) and previously classified as having an enriched MORB-like character (Dadd et al. 2015). However, due to sample

alteration this MORB-like interpretation is ambiguous and the basalt geochemistry could equally be interpreted as having a component of continental contamination. Overall, our observations question whether the CAP is unambiguous oceanic crust, and we suggest it could instead comprise a spectrum of crustal types, ranging from heavily intruded continental crust of the Cuvier Margin to fully magmatic crust generated in sub-aerial or shallow-water environments. If our proposal that the CAP is COTZ is correct, the landward limit of unambiguous oceanic crust adjacent to the Cuvier Margin may be located >500 km further offshore: this would have implications for plate tectonic reconstructions involving the NW Australian margin (cf. Heine & Müller 2005; Gibbons et al. 2012), as well as for heat flow and basin modelling studies. More generally, our study supports previous suggestions that magnetic stripes may not be a unique feature of oceanic crust.

**Continent-Ocean Transition Zone (COTZ) formation**

COTZs at magma-rich passive margins are typically characterised by seismically isotropic, acoustically fast wavespeed (>7 km $s^{-1}$) crust, overlain by SDR lava sequences emplaced within sub-aerial or shallow-water environments (e.g., Eldholm et al. 1989; Larsen & Saunders 1998; Symonds et al. 1998; Menzies et al. 2002). Observations from rifted margins and active rifts suggest that these COTZs are marked by a compositional and structural spectrum, bounded by unambiguous continental and oceanic crust end-members (Fig. 2). From the landward limit of COTZs, we expect the proportion of magma intruded into continental crust to increase oceanwards (Fig. 2) (e.g., Eldholm et al. 1989; Keranen et al. 2004; Daniels et al. 2014). As dyking localises, eventually no continental crust will remain (i.e. break-up of continental crust), and the COTZ will solely comprise igneous intrusions and extrusions emplaced along magmatic segments during sub-aerial or shallow-water extension (Fig. 2) (e.g., Collier et al. 2017; Paton et al. 2017; McDermott et al. 2018); this so-called

magmatic crust is similar to oceanic crust but does not form by deep-marine spreading at a mid-ocean ridge and may be underlain by continental lithospheric mantle. Decay of the buoyant support of these dense, sub-aerial or shallow-water magmatic segments will promote their subsidence (e.g., Corti et al. 2015; McDermott et al. 2018). As these magmatic segments subside to water depths of ≳2 km, plate-spreading drives the generation of unambiguous oceanic lithosphere, the crust of which in magma-rich, fast-spreading areas (>4 cm yr-1 spreading rates; Cannat et al. 2019), like that characterising the CAP, is expected to comprise layers of pillow basalts, sheeted dykes, and gabbro (e.g., McDermott et al. 2018). Across COTZs and into unambiguous oceanic crust, we therefore expect an oceanwards reduction in the continental signature of magma chemistry as they become more MORB-like (Fig. 2). Because of uncertainties in data resolution and interpretation, it is often difficult to constrain the position from heavily intruded continental crust to the onset of magmatic crust emplacement. We therefore combine these domains and refer to them both as a COTZ (Fig. 2).

## Geological Setting

### *Crustal Structure and Age*

The ~400 km wide Gascoyne and 180 km-wide Cuvier margins, which are separated by the NW-trending Cape Range Fracture Zone, form part of the NW Australian magma-rich passive margin (Fig. 1A). This passive margin is bound by the Argo Abyssal Plain to the north, and the Gascoyne Abyssal Plain and Cuvier Abyssal Plain (CAP) to the west (Fig. 1A) (Longley et al. 2002; Stagg et al. 2004). Margin formation occurred during multiple phases of Permian-to-Late Jurassic rifting, culminating in Early Cretaceous break-up of the Gascoyne and Cuvier margin rift segments from Greater India (Fig. 3A) (Longley et al. 2002). A 200–250 km wide COTZ (i.e. the Gallah Province) has been interpreted along the Gascoyne

Margin to consist of a seismically high-velocity lower crust, overlain by 2–5.5 km thick SDR sequences, which overall record M-series magnetic anomalies M10N–M5n (~136–131 Ma, Valanginian-to-Hauterivian; Figs 1A and B) (Symonds et al. 1998; Robb et al. 2005; Direen et al. 2008; Rey et al. 2008); some recent studies have assumed the Gallah Province comprises oceanic crust but have not justified why a COTZ origin is dismissed (e.g., Fig. 1C) (e.g., Gibbons et al. 2012). If the Gallah Province is a COTZ and thus marks the final stages of continental break-up and, the identification of magnetic chron M3n within unambiguous oceanic crust of the adjacent Gascoyne Abyssal Plain indicates that full continental lithospheric rupture and oceanic seafloor spreading occurred by ~130 Ma (Hauterivian; Figs 1B and 3A) (Robb et al. 2005; Direen et al. 2008). Along the Cuvier Margin, beneath the modern continental slope, seismically imaged SDR sequences have previously been interpreted to mark a COTZ, albeit only 50–70 km wide (e.g., Figs 1A and D) (Hopper et al. 1992; Symonds et al. 1998). Based on recognition of at least magnetic chron at least M10N–M10 within the adjacent CAP it has been classified as oceanic crust that started forming at ~136–134 Ma (Valanginian; Figs 1B and 3A) (e.g., Falvey & Veevers 1974; Larson et al. 1979; Robb et al. 2005; Gibbons et al. 2012). If the CAP comprises oceanic crust, these age constraints on its formation suggest full continental lithospheric rupture of the Cuvier Margin occurred ~4–6 Myr before the Gascoyne Margin (Fig. 3A).

*Cuvier Abyssal Plain structure, magnetics, and chemistry*

The CAP lies ~5 km below sea level and comprises a ~6–10.5 km thick crystalline crust (e.g., Fig. 1D) (Hopper et al., 1992). The CAP is bound to the SW by the Wallaby Plateau and Wallaby Saddle, and within the CAP are two linear, NE-trending bathymetric highs that are co-located with linear magnetic anomalies: the Sonne Ridge and Sonja Ridge (Figs 1A and B). Robb et al. (2005) interpreted the magnetic anomalies southeast of the Sonne Ridge as

M10N–M6 (135.9–131.7 Ma) and conjugate to a more poorly developed set of anomalies northwest of the ridge (Fig. 1B). These magnetic anomalies to the NW of the Sonne Ridge, which terminate against the Cape Range Fracture Zone, are cross-cut by at least chron M5n? (131.7–130.6 Ma) either side of the Sonja Ridge (Fig. 1B) (Robb et al. 2005). Based on mapping of these chrons across the CAP, Robb et al. (2005) interpreted the Sonne and Sonja ridges as oceanic spreading centres. Geochemical analyses of a basalt dredged from the Sonne Ridge along its extension into the Wallaby Plateau, suggest it has a slightly enriched MORB-like signature, supporting the inference that the Sonne Ridge is an oceanic spreading centre (Dadd et al. 2015). An alternative interpretation forwarded for the Sonne Ridge is that it represents a 'pseudofault' (i.e. an apparent offset in magnetic stripes formed by ridge jumps; Hey 1977) separating oceanic crust to the SE from a north-eastern extension of the 'part-continental' Wallaby Plateau (Fig. 1C); this interpretation is based on changes in gravity intensity across the structure and the possible termination of the Cape Range Fracture Zone directly north of the ridge (Gibbons et al. 2012). In their model, Gibbons et al. (2012) define a different oceanic spreading centre, located ~100 km to the SE and parallel to the Sonne Ridge, interpreted to be bordered by conjugate chrons M10–M8 (134.2–132.5 Ma) (Fig. 1C). Gibbons et al. (2012) considered the Sonja Ridge to be an oceanic spreading centre, which produced oceanic crust potentially recording chrons M7–M4, isolated within the Wallaby Plateau (Fig. 1C). Beyond the CAP, chron M4 or M3n is the first to occur continuously along-strike across both the Cuvier and Gascoyne margin segments (Figs 1B and C).

*The Wallaby Plateau and Wallaby Saddle*

The Wallaby Plateau is a large bathymetric high (Figs 1A-C), containing up to ~7.5 km thick sequences of volcanic and sedimentary rocks, which are typically expressed in seismic

reflection data as packages of diverging and dipping reflections that appear similar to SDRs (e.g., Colwell et al. 1994; Daniell et al. 2009; Stilwell et al. 2012; Olierook et al. 2015). Interpretation of seismic reflection and magnetic data, coupled with chemical, geochronological, and biostratigraphic analyses of dredge samples, suggests the Wallaby Plateau probably comprises ~124 Myr old, continental flood basalts and interbedded sedimentary strata emplaced on a fragment of extended continental crust (see Olierook et al. 2015 and references therein). Between the Wallaby Plateau and the Australian continent is the Wallaby Saddle, a bathymetric low containing SDRs but no magnetic stripes, interpreted by Symonds et al. (1998) to comprise 'transitional' crust (i.e. non-oceanic; Figs 1A and B). The Wallaby Plateau and Wallaby Saddle seemingly preserve a range of crustal types typical of a COTZ, but not unambiguous continental crust or unambiguous oceanic crust.

***Sedimentary Cover on the Cuvier Abyssal Plain***

The top of the crystalline basement within the CAP corresponds to a high-amplitude reflection in seismic data, which is overlain by a ~1–3.3 km thick, sedimentary succession broadly comprising sub-horizontal reflections (e.g., Fig. 1D) (e.g., Veevers & Johnstone 1974; Hopper et al. 1992). Biostratigraphic and lithological data for the sedimentary cover are available from the DSDP Site 263 borehole, which was drilled in 1972 and terminates ~100–200 m above the basement (Figs 1A and 3B) (e.g., Bolli 1974; Scheibnerová 1974; Wiseman & Williams 1974; Holbourn & Kaminski 1995). These data provide an important record of subsidence history of the Cuvier Abyssal Plain. The lowermost 546 m of strata penetrated by DSDP Site 263 comprise black claystones, which become silty and contain abundant kaolinite towards the base of the borehole (Fig. 3B) (Robinson et al. 1974; Compton et al. 1992). In places, particularly at the base of DSDP Site 263, these silty claystones are poorly sorted and contain angular quartz grains (Robinson et al. 1974).

Analyses of benthic foraminifera from DSDP Site 263 suggest the black, kaolinitic claystones are likely Hauterivian-to-Middle Barremian in age, passing upwards into Albian-to-Aptian black claystones (Fig. 3B) (Holbourn & Kaminski 1995); these age ranges are supported by dinoflagellate distributions and carbon isotope stratigraphy (Wiseman & Williams 1974; Oosting et al. 2006). A gradual upwards transition from coarsely to finely agglutinated foraminifera species, coupled with an upwards increase in the scarcity of shallow-water taxa (e.g., *Hyperamina* spp.) and a corresponding decrease in grain size, suggests that the Hauterivian-to-Middle Barremian strata record deepening neritic (i.e. <200 m water depth) conditions (e.g., Fig. 3B) (Robinson et al. 1974; Veevers & Johnstone 1974; Holbourn & Kaminski 1995; Oosting et al. 2006). Sedimentary rocks recovered from the Pendock-1 borehole, which is located on the Cuvier Margin continental shelf, are sedimentologically similar and of comparable age to those penetrated in DSDP 263 (Veevers & Johnstone 1974; Holbourn & Kaminski 1995). These similarities to Pendock-1 suggest that the Hauterivian-to-Middle Barremian strata sampled by DSDP Site 263 can broadly be correlated to the Winning Group of the North and South Carnarvon basins and likely do not contain products of mass-wasting from the continental slope (Fig. 3) (Veevers & Johnstone 1974; Holbourn & Kaminski 1995).

## Dataset and methodology

### *Seismic reflection data*

To assess the crustal structure of the CAP and surrounding areas, we interpret seven 2D seismic lines from four, pre-stack time-migrated reflection surveys (Fig. 1A) (see Supplementary Table 1 for acquisition and processing details for each survey). Seismic lines EW0113-5, EW0113-6, and repro-n303 are each >400 km long and extend across parts of the Cuvier Margin and the CAP; EW0113-5 and EW0113-6 span the mapped area of SDRs in the

Cuvier COTZ (Hopper et al. 1992) and the location of the extinct spreading centre proposed by Gibbons et al., (2012), whereas repro-n303 images the Sonne Ridge (Fig. 1A). Due to extreme amplitude contrasts between the shallow and deep sections of the original migrated, EW0113 data, we applied a time-dependent gain filter and root filter to improve amplitude balance and enhance deep reflectivity (see supplementary information for details). Lines s135-05, s135-08, and s310-59 image the inferred 'transitional' crust of the Wallaby Saddle and the intruded continental crust of the Wallaby Plateau (e.g., Symonds et al., 1998; Goncharov and Nelson, 2012; Olierook et al., 2015). The NE-trending seismic line s135-11 was also interpreted as it ties together the margin-orthogonal seismic lines and provides a margin-parallel image of the southernmost Exmouth Plateau continental crust, the CAP, and the Wallaby Plateau (Fig. 1A).

Although time-migrated seismic reflection data allows us to qualitatively and quantitatively characterise crustal structure, seismic velocity information is required to convert depth information from seconds two-way time (TWT) to metres. To provide context for the thicknesses and depths of some discussed structures, we depth-converted the EW0113-5 and EW0113-6 seismic data using interval velocities derived from ocean-bottom seismometer (OBS) data (Table 1) (Tischer 2006). The OBS array comprised 20 instruments spaced ~16 km apart and was co-located with seismic line EW0113-6, which is situated ~70 km along-strike from line EW0113-5 (Fig. 1A); the geological structure imaged in line EW0113-6 is very similar to that of EW0113-5, supporting the use of velocities from EW0113-6 to depth convert both lines. As velocity data from across the Wallaby Plateau and Wallaby Saddle is limited (Goncharov & Nelson 2012), and because along-strike variation in geology will likely promote changes in the velocity structure, lines s135-05, s135-08, and s310-59 are presented in time. For easier comparison between seismic data from the CAP and the Wallaby Plateau and Wallaby Saddle, we do not depth-convert repro-n303 or s135-11.

Interpretation of reflection configurations (e.g., dip values) in time-migrated data are only qualitative, and may change if depth-converted.

***Magnetic data***

To examine the regional magnetic anomalies, we utilise the EMAG2v2 and EMAG2v3 Earth Magnetic Anomaly Grids (Maus et al. 2009; Meyer et al. 2017). EMAG2v2 is a 2 arc min resolution grid derived from marine, airborne, and satellite magnetic data, but uses *a priori* information to interpolate magnetic anomalies in areas where data gaps are present (Fig. 4A) (Maus et al. 2009; Meyer et al. 2017). In contrast, EMAG2v3 uses more data points to derive magnetic anomaly maps but assumes no *a priori* information (Fig. 4B) (Meyer et al. 2017). In ocean basins with a relatively poor coverage of magnetic data available, such as the CAP, clear linear magnetic anomalies in EMAG2v2 thus typically appear poorly developed or are absent in EMAG2v3 (cf. Figs 4A and B) (Meyer et al. 2017). This difference in the presence and appearance of linear magnetic anomalies between grids is because (assumed) knowledge of seafloor spreading processes was incorporated into, and therefore influenced, interpolation during construction of the EMAG2v2 grid (Maus et al. 2009; Meyer et al. 2017). Importantly, the apparent reduction in magnetic stripes observed in EMAG2v3, compared to EMAG2v2 (Figs 4A and B), does not necessarily mean these features are absent, but rather that the available data is insufficient to unambiguously confirm their presence in non-directionally gridded data such as EMAG2v3 (Meyer et al. 2017). Comparing the EMAG2v2 and EMAG2v3 grids with shiptrack magnetic data (Robb et al. 2005) allows us to interrogate the magnetic architecture of the CAP (cf. Meyer et al. 2017). In particular, we interpret the EMAG2v2 data by picking the young end of the positive anomaly peaks (Fig. 1B), and compare the defined anomalies to those observed in the EMAG2v3 grid and shiptrack magnetic data. From these comparisons, we tied interpreted magnetic stripes to seismic line

EW0113-5, EW0113-6, and repro-n303 using the synthetic profiles of Robb et al. (2005). To update the absolute ages of the interpreted magnetic anomalies (Robb et al. 2005), we use the time-calibrated, magnetic polarity reversal sequence of Gradstein & Ogg (2012).

***Geochemical data***

To evaluate whether the Sonne Ridge is an extinct seafloor spreading centre (e.g., Mihut & Müller 1998; Robb et al. 2005) consisting of oceanic crust with a MORB or MORB-like affinity along its length, we examine chemical data from a dredged, altered basalt lava sample collected along its extension into the Wallaby Plateau (i.e. Site 57 - sample 057DR051A; diamond 57 in Fig. 1A) (Daniell et al. 2009; Dadd et al. 2015; Olierook et al. 2015). We compare the Sonne Ridge sample to two samples collected from near the south-western margin of the Wallaby Plateau (diamonds 55 and 52 in Fig. 1A) (i.e. Site 55 - samples 055BS004A and 055BS004B) (Dadd et al. 2015). Two Wallaby Plateau basalts dated from Site 52 (Fig 1A) yield plagioclase $^{40}Ar/^{39}Ar$ plateau ages of 125.12±0.9 Ma and 123.80±1.0 Ma, whereas two analyses of the Sonne Ridge sample yielded less precise ages of 120±14 Ma and 123±11 Ma (Olierook et al. 2015).

## Results

***Reflection seismology***

*Cuvier Abyssal Plain*

We interpret a prominent, continuous, high-amplitude seismic reflection across the CAP; this represents the interface between crystalline rock and overlying sedimentary strata (e.g., Figs 1D and 5). The Moho was picked at the base of a sub-horizontal zone of moderate-to-high-amplitude, discontinuous seismic reflections, that coincides with a downwards increase in seismic velocity from ~7.2 km $s^{-1}$ to 8 km $s^{-1}$ and is broadly flat-lying at ~16–17 km or ~10 s

TWT (Fig. 5; Table 1). On EW0113-5, the Moho appears to become shallower oceanwards (to depths ≤14 km), although our interpretation of repro-n303 suggests it may deepen again beneath the Sonne Ridge (Figs 5A and D). Overall, the crystalline crust is ~8–10 km (~3–5 s TWT) thick and is thickest at the Sonne Ridge where crystalline rock is elevated above the adjacent sedimentary cover (Figs 1D and 5). In contrast to the appearance of the Sonne Ridge, there is no evidence of crustal thickening or elevated basement where the spreading ridge proposed by Gibbons et al., (2012) is expected on lines EW0113-5 and EW0113-6 (Figs 1A, C, and 5).

From our seismic reflection data we sub-divide the CAP crust into three distinct seismic facies (Figs 5-8). Across the CAP, the ~1–3 km-thick, uppermost crystalline crustal layer comprises a layered, moderate- to high-amplitude seismic facies (SF1; Fig. 5). On NW-trending seismic lines orthogonal to the margin (i.e. EW0113-5, EW0113-6, and repro-n303), SF1 locally contains ≤40 km wide, ≤4.5 km thick wedges of coherent, high-amplitude, dipping reflections that predominantly diverge seaward (Figs 5 and 6); adjacent to the Sonne Ridge on its NW side, a package of dipping reflections diverge landwards (Fig. 5D). There is no correlation between the location and width of these wedges relative to the magnetic chrons; e.g., some packages of seaward-diverging reflections span several chrons (Fig. 5). Where well-developed wedges are absent, SF1 contains discontinuous, horizontal to gently seaward-dipping reflections (Fig. 5). On line s135-11, which is oriented parallel to the margin, most reflections within SF1 are either sub-horizontal or dip gently north-eastwards (Fig. 7). Seismic velocities for SF1 are estimated to be ~4–5 km/s (Fig. 5; Tischer 2006).

In places, the uppermost crystalline layer (SF1) is underlain by a low-amplitude, near transparent seismic facies (i.e. SF2), which is particularly clear on lines EW0113-5 and EW0113-6 (Figs 5 and 6). SF2 is up to ~2.8 km thick, being thinnest and occasionally absent beneath wedges of dipping reflections within SF1 (Figs 5 and 6). The few reflections that

occur within SF2 typically have low-to-moderate to amplitudes and variable dips (Figs 5 and 6). On repro-n303, at the seaward termination of an overlying wedge in SF1, a ~15 km wide swarm of landward-dipping reflections are present in SF2 (Fig. 5D). There is no clear SF2 observed on line s135-11, even in areas where it is encountered on the intersecting margin-orthogonal lines (Fig. 7).

Beneath SF2 we recognise a ~3.5–6 km (<2 s TWT) thick, low-amplitude layer that locally contains prominent, high-amplitude, dipping reflections and discontinuous, moderate amplitude, sub-horizontal reflections (SF3; Figs 5–7). On line EW0113-5, the inclined reflections within SF3 terminate at the Moho and primarily dip oceanwards at 20–30° (Fig. 5A). On lines EW0113-6 and repro-n303, however, reflections within SF3 dip both oceanwards and landwards (Figs 5B, C, and 6). Mapped reflections within SF3 on s135-11 primarily dip towards the SE, extending from the top of the layer down into the mantle, cross-cutting but not offseting NE-dipping, gently inclined reflections (Fig. 7). Similar mid- and lower-crustal reflection configurations to SF2 and SF3, respectively, occur in the seismic data presented by Hopper et al. (1992) (Fig. 1D). Seismic velocities of SF2 and SF3 are 6.8–7.2 km/s (Fig. 4; Tischer 2006).

*Wallaby Plateau and Wallaby Saddle*

Building on previous investigations of seismic data across the continental-to-COTZ crust of the Wallaby Plateau and Wallaby Saddle, here we (re)interpret several 2D seismic lines and compare their structure to that of the CAP. Similar to the CAP, a prominent, continuous, high-amplitude seismic reflection marks the interface between crystalline rock and overlying sedimentary strata across the Wallaby Plateau and Wallaby Saddle (Figs 7 and 8). Within the Wallaby Saddle, the crust appears to be ~5–6 s TWT thick, although the Moho can only tentatively be interpreted, and can also be sub-divided into: (i) SF1, itself containing up to ~4

s TWT thick, 12 km wide wedges of diverging reflections that typically dip seawards; (ii) restricted zones that are broadly transparent, with some low-to-moderate to amplitude reflections with variable dips, similar to SF2 described from the CAP; and (iii) a 1.5–3 s TWT thick SF3 unit that contains reflections with variable dips, including prominent swarms of landward-dipping reflections that cross-cut but do not offset other reflections and that typically occur at the oceanward termination of SF1 wedges (Fig. 8). Derivation of interval velocities from seismic reflection stacking velocities suggests rocks comprising SF1 have velocities of ~2.5–5.3 km $s^{-1}$ (see insets in Fig. 8C) (Goncharov & Nelson 2012). It is difficult to determine whether SF1-SF3 continue across the full extent of the Wallaby Saddle in s310-59 because across its western portion there appears to be a distinct change in reflection configuration (Fig. 8C). In particular, we observe that although there is less reflectivity in this western portion, reflections towards the top of the crust are broadly sub-parallel to the basement reflection and those within the mid- to lower-crustal areas are either gently inclined landwards, or moderately inclined oceanwards (Fig. 8C).

Seismic reflection imaging of the Wallaby Plateau reveals the crust is up to ~7 s TWT thick (e.g., at the Sonne Ridge), apparently thicker than that of the Wallaby Saddle (~5–6 s TWT thick) but that there is no apparent significant change in Moho depth between the two crustal domains (Figs 7 and 8); we note these observations are based on time-migrated data and may thus be invalidated if there are differences in velocity structure between the two areas not previously recognised. The crust of the Wallaby Plateau is also thicker than that of the CAP, and its underlying Moho is located at deeper levels (~12 s TWT; Fig. 7). Towards the SW margin of the Wallaby Plateau, a ~40 km wide, apparently NE-trending rift system occurs, comprising normal faults with throws of up to ~1 s TWT that bound and dissect a graben (Figs 8B–D). Reflections within the upper section of the Wallaby Plateau crust are typically moderate-to-high amplitude and form layered packages, which are either

conformable to the top basement horizon or that diverge (Fig. 8). The diverging packages of dipping reflections appear similar to SF1 observed in the CAP and Wallaby Saddle (Figs 5 and 8). Derivation of interval velocities from seismic reflection stacking velocities suggests rocks comprising these diverging reflector sequences have velocities of ~2.5–5.3 km $s^{-1}$ (Fig. 8C) (Goncharov & Nelson 2012). Due to uncertainties regarding the reliability of seismic processing within the middle and lower crustal sections of the Wallaby Plateau, e.g., where imaging is hindered by seabed multiples, it is difficult to confidently interpret reflections as real geological features and not artefacts. However, we note that in these middle and lower crustal sections, reflections are low-to-moderate amplitude and broadly dip gently in various directions; in places, steeply inclined reflections are observed that appear to cross-cut but not offset gently dipping reflections (Fig. 8). These steeply inclined mid- to lower-crustal reflections typically appear to be located beneath diverging reflection packages, or beyond their down-dip termination (Fig. 8).

***Comparison of magnetic anomalies to seismic reflection data***

EMAG2v2 and ship-track magnetic data reveal that 10 km wide, ≤220 km long magnetic stripes cover much of the CAP (Figs 1B, C, 4, and 5). No magnetic stripes can confidently be identified and dated within the Wallaby Plateau and none are observed within the Wallaby Saddle (Figs 1B, C, and 4). Although magnetic anomalies in the EMAG2v3 grid are suppressed relative to EMAG2v2, subtle, linear anomalies can still be distinguished across the CAP and in the Gallah Province (cf. Figs 4A and B). Because we identify no ridge-like feature where Gibbons et al. (2012) inferred an extinct seafloor spreading centre, we discard their assignation of magnetic chron ages and instead compare our seismic reflection data to those of Robb et al. (2005). In particular, proximal to the Australian continent, long-wavelength magnetic anomalies can only be broadly assigned to chron M10N (~135.9–134.2

Ma; Figs 1B, 4, and 5) (Robb et al. 2005); across parts of seismic lines EW0113-5, EW0113-6, and repro-n303, chrons M10n–M5r (~135.3–131.4 Ma) are clearly defined and have amplitudes of ≤±100 nT (Figs 1B, 4, and 5). There is no apparent correlation between the distribution of seaward-dipping reflector sequences in SF1 or thickness variations in any of the three seismic facies to the location or intensity of the magnetic chrons (Fig. 5). However, we note that on all three seismic lines, chrons M8r–M7n (~133–132 Ma) coincide with a package of seaward-dipping reflectors observed in SF1, which on EW0113-5 is ≤3 km thick and ~25 km long (Fig. 5). Furthermore, our comparison also shows that individual seaward-dipping reflector sequences can extend across multiple magnetic chrons (Fig. 5).

### *Geochemistry of basalts dredged from the Sonne Ridge*

The only basalt collected from the Sonne Ridge displays a relatively flat Rare Earth Element (REE) pattern and has been previously described as having a slightly enriched MORB-like source (Fig. 9A) (Dadd et al. 2015). By replotting the trace element and radiogenic isotopic compositions of the altered Sonne Ridge sample, we show the sample: (i) displays prominent enrichments in Rb, K, and Pb relative to average enriched MORB (Fig. 9A); (ii) a depletion of Nb relative to average enriched MORB (Fig. 9A); and (iii) an elevated $^{87}Sr/^{86}Sr$ and unradiogenic $\varepsilon_{Nd}$ (Fig. 9B). We also note that the REE pattern defined by the Sonne Ridge basalt appears similar to REE profiles of basalts from the Wallaby Plateau, Globally Subducting Sediment (GLOSS), and average continental crust (Fig. 9A).

## Interpretation

### *Seismic facies*

Beneath the sedimentary cover across the CAP, we recognise three distinct layers (SF1–SF3; Figs 5–8). We identify a upper-crustal layer (SF1) in the CAP that comprises well-developed

wedges of divergent, seaward-dipping reflectors (SDRs) (Figs 5 and 6). These SDRs are ≤4.5 km thick, likely have OBS-derived seismic velocities of ~4–5 km $s^{-1}$ (Tischer 2006), and collectively extend >300 km west of the previously interpreted oceanward limit of the Cuvier Margin COTZ (Figs 1A, 5, and 6). Diverging SDRs are also observed within: (i) the previously defined, 50–70 km wide COTZ along the Cuvier Margin beneath the continental slope, where they are up to ~5 km thick (e.g., Fig. 1D) (e.g., Hopper et al. 1992; Symonds et al. 1998); and (ii) across the Wallaby Saddle and Wallaby Plateau, where they are ~5–10 km thick and have seismic stacking velocities of 2.5–5.3 km $s^{-1}$ (Fig. 8) (e.g., Symonds et al. 1998; Sayers et al. 2002; Goncharov & Nelson 2012). The lack of boreholes penetrating these SDR sequences offshore NW Australia means we cannot determine their composition or the nature of underlying crust. However, SDR sequences that are geometrically and geophysically similar to those from offshore NW Australia (e.g., SF1) have been recognised along other passive margins, where they are developed on either heavily intruded continental crust or thickened oceanic crust (e.g., Hinz 1981; Larsen & Saunders 1998; Harkin et al. 2020). Where these SDRs have been drilled, or are exposed onshore (e.g., Iceland and Greenland), they comprise interbedded basaltic lavas, tuffs, and sedimentary rocks formed during sub-aerial, or perhaps shallow-water, continental breakup and crustal spreading (e.g., Bodvarsson & Walker 1964; Mutter et al. 1982; Roberts et al. 1984; Eldholm et al. 1987; Larsen et al. 1994a; Geoffroy et al. 2001; Harkin et al. 2020). Based on similarities in structure and seismic velocities to SDRs studied elsewhere, we suggest that SF1 comprises spreading-related volcanic rocks interbedded with sedimentary layers (Figs 1D, 5, 6, and 8) (e.g., Mutter et al. 1982; Hopper et al. 1992; Symonds et al. 1998; Planke et al. 2000; McDermott et al. 2019; Harkin et al. 2020).

The observed structure and seismic velocities (6.8–7.2 km $s^{-1}$) of SF2 and SF3 in the CAP, defined by transparent seismic facies and discordant high-amplitude reflections,

451 respectively (Figs 5–8), are consistent with the typical seismic character of sheeted dykes and
452 lower crustal gabbro intrusions in oceanic crust (e.g., Eittreim et al. 1994; Paton et al. 2017).
453 However, we note that these seismic facies are not uniquely diagnostic of oceanic crust but
454 can also occur in COTZs, where moderate- to high-amplitude reflections may represent
455 igneous intrusions (e.g., dykes and sills), primary layering within gabbros, or texturally
456 distinct lower crustal shear zones within otherwise homogenous crystalline rocks (e.g.,
457 Phipps-Morgan & Chen 1993; Abdelmalak et al. 2015; Paton et al. 2017). For example, the
458 swarm of landward dipping reflections within SF2 and SF3 at the down-dip termination of an
459 SDR sequence may correspond to dykes; i.e. they cross-cut but do not offset background
460 reflections and are thus not faults or shear zones (e.g., Figs 5 and 8) (e.g., Abdelmalak et al.,
461 2015; Phillips et al., 2018).
462
463 ***Geochemistry of basalts dredged from the Sonne Ridge***
464 Given the Sonne Ridge basalt displays a relatively flat REE profile (Fig. 9A), Dadd et al.
465 (2015) interpreted it to have a slightly enriched MORB-like source and thus supported the
466 inference that the CAP comprises oceanic crust (e.g., Larson et al. 1979; Hopper et al. 1992;
467 Mihut & Müller 1998). Although a flat REE pattern can be indicative of a garnet-free melting
468 regime, such as where a majority of melt is generated in a MORB setting, it does not preclude
469 other settings. It should be noted that the Sonne Ridge submarine sample is heavily altered
470 (Dadd et al. 2015), which may explain the observed elemental enrichment in fluid mobile
471 elements such as Pb and Rb, as well as its elevated $^{87}Sr/^{86}Sr$. However, the sample also
472 exhibits unradiogenic $\varepsilon_{Nd}$ outside the isotopic compositions typical of MORB (Fig. 9B), and a
473 negative anomaly in the fluid immobile, high field strength element Nb, which is in part
474 defined by a relative enrichment in the neighbouring element Th. It is plausible that the
475 negative Nb anomaly and unradiogenic $\varepsilon_{Nd}$ may indicate a chemically evolved, continental or

476 sedimentary contribution to the magmas. Furthermore, the chemical similarity of the Sonne
477 Ridge basalt to two ~124 Ma samples from the Wallaby Plateau (Fig. 9), which is interpreted
478 to comprise intruded continental crust (Daniell et al. 2009; Stilwell et al. 2012; Olierook et al.
479 2015), could be considered consistent with a continental or sedimentary contribution to the
480 Sonne Ridge magmas. Overall, our reinterpretation of the single available, highly altered
481 basalt from the Sonne Ridge highlights that its chemistry does not provide conclusive
482 evidence for the origin of the CAP (cf. Dadd et al. 2015).
483
484 **Discussion**
485 Since its magnetic stripes were identified, the CAP has been considered to comprise
486 unambiguous oceanic crust that formed at ~136–134 Ma (Valanginian) in response to
487 seafloor spreading at the Sonne Ridge (e.g., Fig. 10A) (e.g., Falvey & Veevers 1974; Larson
488 et al. 1979; Hopper et al. 1992; Robb et al. 2005; Gibbons et al. 2012). An oceanic origin for
489 the CAP has been supported by seismic reflection-based observations that it has a thin crust
490 relative to adjacent continental blocks (e.g., Fig. 1D) (e.g., Hopper et al. 1992), and chemical
491 data, which suggest it has a MORB-like signature (Dadd et al. 2015). The apparent certainty
492 that the CAP is oceanic means it has been unquestionably treated as such in all geological
493 models of the evolution of NW Australia, including regional and global plate kinematic
494 reconstructions (e.g., Heine & Müller 2005; Gibbons et al. 2012). However, the identification
495 of linear magnetic anomalies within non-oceanic crust, in areas such as Ethiopia and the
496 Atlantic margins (e.g., Bronner et al. 2011; Bridges et al. 2012; Collier et al. 2017;
497 McDermott et al. 2018), prompts a reassessment of the nature of the crust defining the CAP.
498
499 ***Implications of SDR recognition for the CAP***
500 *Origin of SDR lavas*

Lavas within SDR wedges are inferred to emanate from and be thickest at axial magmatic segments, where they are likely fed by sub-vertical dykes (e.g., Abdelmalak et al. 2015; Norcliffe et al. 2018). With continued plate divergence, these lavas subside and rotate to dip inwards towards their eruption site (e.g., Planke & Eldholm 1994; Paton et al. 2017; Norcliffe et al. 2018; Tian & Buck 2019); this subsidence also rotates underlying feeder dykes, which will thus dip away from the magmatic segment (e.g., Lenoir et al. 2003; Abdelmalak et al. 2015). SDRs across the CAP appear to dip and diverge north-westwards, except one SDR-like package of concave-upwards reflections that borders and diverges south-eastwards towards the Sonne Ridge; i.e. we define a conjugate set of SDRs that occur either side of and dip towards the Sonne Ridge (Fig. 5). Although only one SDR package to the NW of the Sonne Ridge dips south-eastwards towards the ridge, we suggest that the other SDR packages, which dip north-westwards, relate to and were formed at the Sonja Ridge (Fig. 5). We also note that along EW0113-5 and EW0113-6 there are no changes in SDR divergence direction, as well as no localised increase in crustal thickness or elevated basement, where Gibbons et al. (2012) proposed the CAP spreading ridge was located (Figs 1C, 5A, and B). Given this lack of evidence for a spreading ridge ~100 km SE of the Sonne Ridge, we discount the crustal and magnetic chron configuration of Gibbons et al. (2012), and instead follow that presented by Robb et al. (2005) (cf. Figs 1B, C, and 10A).

Overall, from the SDR geometries and distribution we describe, coupled with the previously inferred conjugate sets of magnetic chrons (Fig. 1B), our results are consistent with suggestions that: (i) extension within the CAP was predominantly centred on the Sonne Ridge during chrons M10N–M5r (~136–131 Ma); before (ii) briefly jumping to the Sonja Ridge at ~131 Ma (chron M5n), which interrupted subsidence and rotation of the SDR wedge immediately to the NW of the Sonne Ridge and instead produced north-westwards diverging SDRs (Falvey & Veevers 1974; Larson et al. 1979; Robb et al. 2005; MacLeod et al. 2017).

Our reinterpretation of the Sonne Ridge basalt indicates its chemical signature cannot be used to conclusively define whether the Sonne Ridge represents an oceanic or intra-COTZ spreading centre (Dadd et al. 2015).

*Environment of SF1 lava emplacement*

Borehole and field data reveal SDR lavas typically erupt sub-aerially, but can develop sub-aqueously (e.g., Bodvarsson & Walker 1964; Mutter et al. 1982; Roberts et al. 1984; Eldholm et al. 1987; Larsen et al. 1994b; Symonds et al. 1998; Planke et al. 2000; Geoffroy et al. 2001; Harkin et al. 2020). Determining the environment and age of SDR formation can help establish whether they likely formed via: (i) seafloor spreading at a mid-ocean ridge, consistent with previous interpretations that the CAP comprises unambiguous oceanic crust (e.g., Falvey & Veevers 1974; Larson et al. 1979; Hopper et al. 1992; Robb et al. 2005); or (ii) magmatic addition along a sub-aerial or shallow-water axis during the transition from continental rifting to full plate separation (e.g., McDermott et al. 2018), implying the CAP does not comprise oceanic crust. However, from their seismic character alone it can be difficult to determine whether SDRs formed in sub-aerial, shallow-water, or deep-marine environments (e.g., compare inner and outer SDR character and inferred emplacement conditions; Symonds et al. 1998; Planke et al. 2000).

Observations from the DSDP Site 263 borehole, which terminates ~100–200 m above the CAP crystalline crust, indicate the sedimentary cover deposited above the SDRs: (i) comprises poorly sorted silty claystones that include angular quartz grains and abundant kaolinite, consistent with a neritic (i.e. <200 m water depth) depositional environment (Fig. 3B) (e.g., Robinson et al. 1974; Veevers & Johnstone 1974; Compton et al. 1992; Holbourn & Kaminski 1995; Oosting et al. 2006); (ii) contain coarsely agglutinated foraminifera species and taxa such as *Hyperamina* spp. within the lowermost intersected strata, which are

typical of shallow-marine conditions (Holbourn & Kaminski 1995); and (iii) based on biostratigraphic data were deposited at least in the middle Barremian (e.g., ~127 Ma), but are perhaps as old as Hauterivian (~132.6–129.4 Ma) (Oosting et al. 2006). As DSDP Site 263 occurs above crust recording chron M10N (135.9–134.2 Ma), these age constraints suggest local deposition of the lowermost sedimentary cover occurred up to ~9 Myr (i.e. ~135.9–127 Ma) later than the underlying basement, concurrent with development of crust hosting chrons M7–M1n (132.5–126.3 Ma). Crust hosting chrons M7–M1n is located >100 km to the NW of chron M10N (Fig. 1B). Critically, SDR-bearing crust cools and subsides as it is transported away from its emplacement site, leading to rotation of the SDR sequence (e.g., Planke & Eldholm 1994; Paton et al. 2017; Norcliffe et al. 2018; Tian & Buck 2019). The presence of strata deposited in the neritic zone above SF1 in DSDP 263, after ~9 Myr of crustal cooling and subsidence, thus implies lava eruption during the early stages of CAP formation occurred: (i) in a sub-aerial or shallow-water environment (i.e. comparable to the inner SDRs of Symonds et al. 1998; Planke et al. 2000), if we assume the underlying crust only subsided in the ~9 Myr between SDR emplacement and sediment deposition; or (ii) at a moderately deep-marine spreading centre (i.e. comparable to the outer SDRs of Symonds et al. 1998; Planke et al. 2000), but localised uplift elevated the DSDP 263 area to bathymetric depths equivalent to the neritic zone prior to deposition of overlying strata. We lack the data from strata directly overlying or interbedded with the SDRs to test these two interpretations regarding lava emplacement depth, but note that the relatively flat-lying crystalline crust across the interpreted CAP seismic lines (except for the Sonne Ridge) provides no evidence of post-spreading uplift, perhaps suggesting a sub-aerial or shallow-water environment of emplacement is most plausible (Fig. 5).

***Nature of CAP crust***

576 Seismic and magnetic data alone are insufficient to determine the origin of the CAP crust
577 because the SDRs, seismic facies (SF1–SF3), and magnetic stripes these data illuminate can
578 manifest in both oceanic crust and COTZs (e.g., Larsen & Saunders 1998; Symonds et al.
579 1998; Planke et al. 2000; Bridges et al. 2012; Collier et al. 2017; McDermott et al. 2018). We
580 also show that the chemical data available for a basalt from the Sonne Ridge may possess a
581 continental signature, and is thus inconclusive regarding whether or not the crust is oceanic
582 (Fig. 9) (cf. Dadd et al. 2015). Instead, based on lithological and biostratigraphic data from
583 the sedimentary cover intersected by DSDP Site 263, we suggest it may be possible that: (i)
584 the inferred lavas within SF1, at least during the early stages of CAP formation (i.e. chron
585 M10N), erupted in a sub-aerial, or perhaps shallow-water (<200 m water depth),
586 environment; and (ii), assuming the underlying crystalline crust had since subsided relative to
587 its formation position, that during deposition of sedimentary cover on crust recording chron
588 M10N, the contemporaneous, ~9 Myr old Sonne Ridge was elevated above at least the base
589 of the neritic zone. These potential constraints on SDR emplacement depth are inconsistent
590 with the CAP being oceanic crust since mid-ocean ridges in such a setting are expected to
591 occur at water depths of ~3 km after 5–10 Myr of spreading (e.g., Menard 1969; Parsons &
592 Sclater 1977; Stein & Stein 1992).

593 From the distribution of the magnetic chrons (Fig. 1B) and the probable sub-aerial or
594 shallow-water elevation of the ridge during extension, we propose currently available
595 information is consistent with the CAP comprising a COTZ (Fig. 10B). In particular, we
596 suggest the CAP could record a gradual north-westwards change from the continental crust of
597 the Cuvier Margin into heavily intruded continental crust, and progressively becomes
598 increasingly magma-dominated towards the Sonne Ridge (Figs 2, 10B, and C). Our data are
599 insufficient to determine where, or if, there is a transition from heavily intruded continental
600 crust to magmatic crust, which would mark break-up of the continental crust within the CAP.

Our proposed alternative model implies that full continental lithospheric rupture may not have occurred in the CAP; we currently lack data constraining the nature of the CAP crust bearing chron M5n adjacent to the Sonja Ridge or detailed enough to mdoel residual bathymetric anomalies to fully test this hypothesis (Figs 10B and C).

Repetition of the M10N-M6 chrons centred on the Sonne Ridge suggests the possible COTZ of the CAP may extend at least out to chron M3n, which is recorded by inferred unambiguous oceanic crust situated: (i) >500 km oceanwards of the outer- limit of the previously defined Cuvier COTZ (e.g., Hopper et al. 1992; Symonds et al. 1998); and (ii) broadly coincident with the north-western limit of the Gallah Province on the Gascoyne margin (Direen et al. 2008) (Figs 1B and 10B). We suggest rupture of the continental lithosphere and onset of seafloor spreading could have occurred simultaneously offshore the Cuvier and Gascoyne margins at ~131 Ma (Hauterivian), following an oceanwards ridge jump from the Sonja Ridge, producing unambiguous oceanic crust recording chron M3n (Figs 10B and C) (e.g., Robb et al. 2005; Direen et al. 2008). Continuation of the COTZ across the CAP has implications for the timing and kinematics of plate reconstructions of the NW Australian margin, with the onset of deep-marine seafloor spreading potentially ~3 Myr later than suggested by previous studies (e.g., Robb et al. 2005).

Interpreting the CAP as a COTZ developed through sub-aerial, or at least shallow-water, extension implies its crust was: (i) thicker during SDR emplacement, but concurrently and/or subsequently thinned during continued magmatic extension and late-stage stretching (e.g., Bastow & Keir 2011; Bastow et al. 2018); (ii) less dense and thus more buoyant than unambiguous oceanic crust, because it likely retained a significant proportion of continental material; and (iii) thermally buoyant due to the presence of abundant hot intrusions and underlying, decompressing mantle. That these processes can maintain rift axes at above or near sea-level elevations is demonstrated by the onshore occurrence of active rift zones,

characterised by heavily-intruded continental crust, in the Main Ethiopia Rift and Afar (e.g., Hayward & Ebinger 1996; Ebinger & Casey 2001; Mackenzie et al. 2005; Bridges et al. 2012).

Because the degree of thermal subsidence is at least partly controlled by crustal density, we would expect oceanic crust to thermally subside more than less dense, heavily-intruded continental crust. Given the Hauterivian-to-Middle Barremian sedimentary strata overlying the SDRs were deposited in neritic conditions (Veevers & Johnstone 1974; Holbourn & Kaminski 1995; Oosting et al. 2006), it is apparent the CAP subsided from near sea-level to a current, unloaded basement depth of ~6.5 km; this total subsidence is greater than predicted for dense, thermally subsiding oceanic crust (Stein & Stein 1992). To interpret the CAP as COTZ crust, our results would require other mechanisms, in addition to thermal subsidence, to influence its subsidence history. For example, post-breakup decay of asthenospheric thermal anomalies may account for some elevation discrepancies via removal of dynamic support of the margin (e.g., Czarnota et al. 2013). Finally, the CAP COTZ may have involved some late-stage stretching prior to terminal breakup and the onset of seafloor spreading, akin to processes observed today in the sub-aerial Red Sea rift in Ethiopia (e.g., Bastow & Keir 2011; Daniels et al. 2014).

***Development of magnetic stripes during break-up***

Recent forward modelling of conjugate, ship-track magnetic profiles by Collier et al. (2017) suggest magnetic signals over SDRs arise from a combination of stacked and rotated lavas, producing a long-wavelength positive anomaly that can sometimes mask reversals, and linear magnetic anomalies caused by dyke intrusion in the underlying crust. Stacked SDR wedges on the CAP are part of a possible COTZ and span several chrons (e.g. M8n-M7r), but are ≤4.5 km thick (Figs 5 and 6). These observations indicate the CAP magnetic stripes likely

record magnetic reversal signatures originating from sub-SDR rocks; i.e. the SDRs and flat-lying lavas are too thin to dominate the magnetic signature (cf. Collier et al. 2017). In contrast¸ the less-clearly developed yet higher amplitude magnetic reversals in the Gallah Province COTZ may relate to interference from the greater SDR thicknesses (≤5.5 km) relative to the CAP (Direen et al. 2008). Our inference that the magnetic signature is derived from sub-SDR rocks is also consistent with studies of onshore incipient spreading centres (e.g. Ethiopia), where magnetic stripes likely originate from axial intrusion by dykes in heavily intruded, upper continental crust, rather than overlying lavas (Bridges et al. 2012).

We suggest that SDR thickness and, thereby, preservation of magnetic anomalies within a COTZ can partly be attributed to extension rate. For example, the extension rate during SDR eruption offshore NW Australia (~4.5 cm/yr half rate; Robb et al. 2005) is substantially faster than the inferred extension rates for the South Atlantic during magmatic crust formation (~1.1 cm/yr half-rate; Paton et al. 2017). Slower extension rates (e.g. South Atlantic) likely promote stacking of lava flows to produce thicker SDRs (Eagles et al. 2015), leading to interference between the magnetic signal of the SDRs and sub-SDR crust and thus the development of the long-wavelength positive magnetic anomalies (e.g., Moulin et al. 2010). Extension rate may also influence magnetic anomaly development by affecting the width of magnetic stripes; reversal anomalies will be narrowest at slow spreading ridges (Vine 1966). The narrower anomalies, combined with the greater potential for vertical stacking of lavas, will tend to hinder the interpretation of magnetic anomalies.

## Conclusions

The recognition of magnetic stripes within the Cuvier Abyssal Plain (CAP), offshore NW Australia, has led to the assumption that it comprises oceanic crust generated by conventional seafloor spreading at the Sonne Ridge, probably at water depths of ≳2 km. We challenge this

assumption, in line with the growing consensus that magnetic stripes are not necessarily diagnostic of oceanic crust and can also form in continent-ocean transition zones (COTZs). Using regional 2D seismic reflection lines we demonstrate that the uppermost layer in the CAP crystalline crust contains seaward-dipping reflector (SDR) sequences, akin to those observed in the previously defined COTZ of the Cuvier Margin and Wallaby Saddle, as well as on the heavily intruded continental crust of the Wallaby Plateau. Through comparison to SDRs recognised elsewhere, we suggest those observed across the CAP comprise lavas, interbedded with sedimentary strata, erupted from an axial magmatic segment. Lithological and biostratigraphic data from a borehole penetrating the CAP sedimentary cover, which were deposited in neritic (<200 m water depth) conditions, require the underlying crystalline crust to have been at shallow-water depths ~9 Myr after its formation and thus imply SDR emplacement occurred in a shallow water or sub-aerial environment. We also reinterpret chemical data from a basalt dredged along the Sonne Ridge, showing it cannot be conclusively attributed to a MORB setting as previously interpreted. Overall, these data and interpretations suggest the CAP may not comprise unambiguous oceanic crust, but could instead represent a >500 km wide COTZ where extension likely became more magma-dominated, producing heavily-intruded continental crust (akin to present-day Ethiopia) at its landward edge through to magmatic crust formed by sub-aerial or shallow-marine spreading at the Sonne and Sonja ridges. In our conceptual model, break-up of the continental crust could have occurred during the formation of the CAP, but full continental lithospheric rupture occurred outboard of the COTZ following a ridge jump at ~130 Ma. Our re-evaluation of the CAP crustal type supports suggestions that COTZs along volcanic passive margins may record the development of magnetic stripes, which thus should not be used alone as a reliable proxy for the onset of seafloor spreading and the extent of oceanic crust.

**Acknowledgements**

Schlumberger are thanked for provision of Petrel software licenses. M.T.R. was supported by NERC grant NE/L501621/L. The EW0113 seismic survey and EMAG2 magnetic anomaly grids were, and can be acquired from, the UTIG Marine Geoscience Data System and the NOAA National Geophysical Data Centre, respectively. Gwenn Peron-Pinvidic, Gareth Roberts, and Saskia Goes are thanked for helpful discussions during the preparation of this manuscript. We thank five reviewers, including Jon Bull, for their constructive comments on previous versions of this manuscript. Finally we are grateful to Amy Gilligan for the editorial handling of this manuscript, and to Lucía Pérez-Díaz and an anonymous reviewer for their constructive comments.

**Figure captions**

Figure 1: (A) Location map of the study area highlighting the seismic lines used in this study and key tectonic elements, including areas of recognised seaward-dipping reflectors (SDRs) (Symonds et al. 1998; Holford et al. 2013) and continent-ocean transition zones (COTZs; Symonds et al. 1998; Direen et al. 2008). Inset: study area location offshore NW Australia. AAP – Argo Abyssal Plain, CAP – Cuvier Abyssal Plain, CRFZ – Cape Range Fracture Zone, GAP – Gascoyne Abyssal Plain, GP – Gallah Province, NCB – North Carnarvon Basin, EP – Exmouth Plateau, PB – Perth Basin, SCB – South Carnarvon Basin, Cu – Cuvier margin COTZ, SR – Sonne Ridge, SjR – Sonja Ridge, WP – Wallaby Plateau, WS – Wallaby Saddle, WZFZ – Wallaby-Zenith Fracture Zone. Dredge sites 52, 55 (samples 055BS004A and 055BS004B), and 57 (sample 057DR051A) are also shown (Dadd et al. 2015). See Supplementary Figure S1 for an uninterpreted version. (B) Total magnetic intensity grid (EMAG2v2), interpreted magnetic chrons based on Robb et al. (2005). See Supplementary Figure S1 for an uninterpreted version. (C) Total magnetic intensity grid (EMAG2v2),

interpreted magnetic chrons based on Gibbons et al. (2012). See Supplementary Figure S1 for an uninterpreted version. (C) Uninterpreted and interpreted seismic line (i.e. seismic profile 670) across the Cuvier Margin, imaging the crustal structure beneath the continental shelf and the deep abyssal plain (modified from Hopper et al., 1992). Velocity profiles from refraction experiments shown; see Hopper et al., (1992) for details. See Figure 1A for approximate line location and Supplementary Figure S2 for an enlarged version of the uninterpreted seismic line.

Figure 2: Schematic model (not to scale) of a continent-ocean transition zone along a magma-rich passive margin, which depicts the evolution from unambiguous continental crust to unambiguous oceanic crust. As magma intrudes continental crust, likely as dykes at mid- to upper-crustal levels and larger gabbroic bodies in the lower crust, it becomes ‘heavily intruded continental crust’ (e.g., Eldholm et al. 1989). Continued intrusion and dyking leads to localisation of magmatism within narrow zones where there is little, if any, continental crust remaining (i.e. 'magmatic crust'; e.g., Collier et al. 2017; Paton et al. 2017). We categorize heavily intruded continental crust and magmatic crust as ‘COTZ crust’. Sub-aerial, magma-assisted rifting may feed extensive lava flows that later, through subsidence, become seaward-dipping reflectors (SDRs). SDR subsidence leads to rotation of underlying dykes (Abdelmalak et al. 2015); a similar rotation of lavas and dykes is observed in oceanic crust (Karson 2019).

Figure 3: Tectono-stratigraphic chart for the Exmouth Plateau and Cuvier Margin (after Hocking et al., 1987; Arditto, 1993; Partington et al. 2003; Willis, 2005; Reeve et al. 2016). (B) Comparison between stratigraphic data from DSDP 263 and Pendock-1 boreholes

750 (modified from Veevers & Johnstone, 1974; Holbourn & Kaminski, 1995). See Figure 1A for
751 borehole locations.
752
753 Figure 4: Total magnetic intensity grids EMAG2v2 and EMAG2v3 (Maus et al. 2009; Meyer
754 et al. 2017), compared with shiptrack magnetic data (Robb et al. 2005). The limits of
755 unambiguous continental crust, locations of previously defined COTZs, possible spreading
756 ridges, and seismic lines also shown (see Fig. 1 for legend).
757
758 Figure 5: Interpreted and uninterpreted, depth-converted seismic lines (A) EW0113-5 and (B)
759 EW0113-6, and the time-migrated line (D) repro n303 showing crustal structure of the Cuvier
760 Margin; see Figures 1A and 5C for line locations. The tie-co-located magnetic anomaly
761 profile showing interpreted magnetic chrons is presented for (A–D) (after Robb et al. 2005).
762 See Supplementary Figure S2 for an enlarged version of the uninterpreted seismic lines.
763
764 Figure 6: Zoomed in view of EW0113-5 highlighting the seismic character of interpreted
765 SDR packages (see Fig. 5A for location).
766
767 Figure 7: Interpreted and uninterpreted, time-migrated seismic line s135-11; see Figure 1A
768 for location. See Supplementary Figure S2 for an enlarged version of the uninterpreted
769 seismic line.
770
771 Figure 8: Interpreted and uninterpreted, time-migrated seismic lines (A) s135-s135_05, (B)
772 s135-08, and (D) s310-59 showing crustal structure of the Wallaby Plateau and Wallaby
773 Saddle; see Figures 1A and 8D for line locations. See Supplementary Figure S2 for an
774 enlarged version of the uninterpreted seismic lines.

Figure 9: (A) Primitive mantle normalized incompatible element diagram comparing the dredged Sonne Ridge and Wallaby Plateau basalt lava samples with average (ave.) compositions of MORB variants (Hofmann 2014), Globally Subducting Sediment (GLOSS) (Plank & Langmuir 1998), and continental crust (Rudnick & Fountain 1995). Primitive mantle normalisation factors from (Sun & McDonough 1989). (B) Plot of $\varepsilon$(Nd) versus $^{87}Sr/^{86}Sr$, illustrating that the Sonne Ridge and Wallaby Plateau samples are distinct from MORB (based on data collated in Hofmann 2014). Both measured and initial $^{87}Sr/^{86}Sr$ ratios are given in Dadd et al. (2015). It is unclear if the reported $^{143}Nd/^{144}Nd$ in Dadd et al. (2015) is age corrected or not. We assume that they are not, and plot both age corrected and measured Sr-Nd isotopic compositions.

Figure 10: (A) Map showing the potential limits of the COTZ based on interpreting the CAP and Gallah Province as transitional and/or magmatic crust. (B-D) Schematic maps showing the development of COTZ crust and the onset of oceanic crust accretion adjacent to the Gascoyne and Cuvier margins, during formation of chrons (B) M10, (C) M6 and (D) M3r. See Figure 1 for chron ages. Location of present day coastline shown for reference.

## References


Abdelmalak, M.M., Andersen, T.B., Planke, S., Faleide, J.I., Corfu, F., Tegner, C., Shephard, G.E., Zastrozhnov, D.*, et al.* 2015. The ocean-continent transition in the mid-Norwegian margin: Insight from seismic data and an onshore Caledonian field analogue. *Geology*, **43**, 1011-1014.

Bastow, I.D. & Keir, D. 2011. The protracted development of the continent-ocean transition in Afar. *Nature Geosci*, **4**, 248-250.

Bastow, I.D., Booth, A.D., Corti, G., Keir, D., Magee, C., Jackson, C.A.L., Warren, J., Wilkinson, J.*, et al.* 2018. The Development of Late-Stage Continental Breakup: Seismic Reflection and Borehole Evidence from the Danakil Depression, Ethiopia. **37**, 2848-2862.

Bodvarsson, G. & Walker, G. 1964. Crustal drift in Iceland. *Geophysical Journal International*, **8**, 285-300.

Bolli, H.M. 1974. *Jurassic and Cretaceous Calcisphaerulidae from DSDP Leg 27, eastern Indian Ocean*.

Bridges, D.L., Mickus, K., Gao, S.S., Abdelsalam, M.G. & Alemu, A. 2012. Magnetic stripes of a transitional continental rift in Afar. *Geology*, **40**, 203-206.

Bronner, A., Sauter, D., Manatschal, G., Péron-Pinvidic, G. & Munschy, M. 2011. Magmatic breakup as an explanation for magnetic anomalies at magma-poor rifted margins. *Nature Geoscience*, **4**, 549.

Cannat, M., Sauter, D., Lavier, L., Bickert, M., Momoh, E. & Leroy, S. 2019. On spreading modes and magma supply at slow and ultraslow mid-ocean ridges. *Earth and Planetary Science Letters*, **519**, 223-233.

Causer, A., Pérez-Díaz, L., Adam, J. & Eagles, G. 2020. Uncertainties in break-up markers along the Iberia–Newfoundland margins illustrated by new seismic data. *Solid Earth*, **11**, 397-417.

Collier, J.S., McDermott, C., Warner, G., Gyori, N., Schnabel, M., McDermott, K. & Horn, B.W. 2017. New constraints on the age and style of continental breakup in the South Atlantic from magnetic anomaly data. *Earth and Planetary Science Letters*, **477**, 27-40.

Colwell, J., Symonds, P. & Crawford, A. 1994. The nature of the Wallaby (Cuvier) Plateau and other igneous provines of the west Australian margin. *Journal of Australian Geology and Geophysics*, **15**, 137-156.

Compton, J., Mallinson, D., Netranatawong, T. & Locker, D. 1992. *Regional correlation of mineralogy and diagenesis of sediment from the Exmouth Plateau and Argo Basin, Northwestern Australian Continental Margin*.

Corti, G., Agostini, A., Keir, D., Van Wijk, J., Bastow, I.D. & Ranalli, G. 2015. Magma-induced axial subsidence during final-stage rifting: Implications for the development of seaward-dipping reflectors. *Geosphere*, **11**, 563-571.

Czarnota, K., Hoggard, M., White, N. & Winterbourne, J. 2013. Spatial and temporal patterns of Cenozoic dynamic topography around Australia. *Geochemistry, Geophysics, Geosystems*, **14**, 634-658.

Dadd, K.A., Kellerson, L., Borissova, I. & Nelson, G. 2015. Multiple sources for volcanic rocks dredged from the Western Australian rifted margin. *Marine Geology*, **368**, 42-57.

Daniell, J., Jorgensen, D., Anderson, T., Borissova, I., Burq, S., Heap, A., Hughes, D., Mantle, D.*, et al.* 2009. Frontier basins of the West Australian continental margin. *Geoscience Australia Record*, **38**, 243.

Daniels, K.A., Bastow, I.D., Keir, D., Sparks, R.S.J. & Menand, T. 2014. Thermal models of dyke intrusion during development of continent–ocean transition. *Earth and Planetary Science Letters*, **385**, 145-153, http://doi.org/http://dx.doi.org/10.1016/j.epsl.2013.09.018.

Direen, N.G., Stagg, H.M.J., Symonds, P.A. & Colwell, J.B. 2008. Architecture of volcanic rifted margins: new insights from the Exmouth – Gascoyne margin, Western Australia. *Australian Journal of Earth Sciences*, **55**, 341-363, http://doi.org/10.1080/08120090701769472.

Direen, N.G., Borissova, I., Stagg, H., Colwell, J.B. & Symonds, P.A. 2007. Nature of the continent–ocean transition zone along the southern Australian continental margin: a comparison of the Naturaliste Plateau, SW Australia, and the central Great Australian Bight sectors. *Geological Society, London, Special Publications*, **282**, 239-263.

Eagles, G., Pérez-Díaz, L. & Scarselli, N. 2015. Getting over continent ocean boundaries. *Earth-Science Reviews*, **151**, 244-265.

Ebinger, C.J. & Casey, M. 2001. Continental breakup in magmatic provinces: An Ethiopian example. *Geology*, **29**, 527, http://doi.org/10.1130/0091-7613(2001)029<0527:cbimpa>2.0.co;2.

Eittreim, S.L., Gnibidenko, H., Helsley, C.E., Sliter, R., Mann, D. & Ragozin, N. 1994. Oceanic crustal thickness and seismic character along a central Pacific transect. *Journal of Geophysical Research: Solid Earth*, **99**, 3139-3145.

Eldholm, O., Thiede, J. & Taylor, E. 1989. The Norwegian continental margin: tectonic, volcanic, and paleoenvironmental framework. *Proceedings of the ocean drilling program, Scientific results*. Citeseer, 5-26.

Eldholm, O., Thiede, J., Taylor, E. & Party, S.S. 1987. Summary and preliminary conclusions, ODP Leg 104. *Proceedings of the Ocean Drilling Program, Scientific Results*. Ocean Drilling Program College Station, Texas, 751-771.

Falvey, D. & Veevers, J. 1974. Physiography of the Exmouth and Scott plateaus, western Australia, and adjacent northeast Wharton Basin. *Marine Geology*, **17**, 21-59.

Geoffroy, L., Callot, J.P., Scaillet, S., Skuce, A., Gélard, J., Ravilly, M., Angelier, J., Bonin, B.*, et al.* 2001. Southeast Baffin volcanic margin and the North American-Greenland plate separation. *Tectonics*, **20**, 566-584.

Gibbons, A.D., Barckhausen, U., den Bogaard, P., Hoernle, K., Werner, R., Whittaker, J.M. & Müller, R.D. 2012. Constraining the Jurassic extent of Greater India: Tectonic evolution of the West Australian margin. *Geochemistry, Geophysics, Geosystems*, **13**.

892 Goncharov, A. & Nelson, G. 2012. From two way time to depth and pressure for interpretation of
893 seismic velocities offshore: Methodology and examples from the Wallaby Plateau on the West
894 Australian margin. *Tectonophysics*, **572**, 26-37.

895
896 Gradstein, F. & Ogg, J. 2012. The chronostratigraphic scale *The geologic time scale*. Elsevier, 31-42.

897
898 Harkin, C., Kusznir, N., Roberts, A., Manatschal, G. & Horn, B. 2020. Origin, composition and relative
899 timing of seaward dipping reflectors on the Pelotas rifted margin. *Marine and petroleum geology*,
900 **114**, 104235.

901
902 Hayward, N. & Ebinger, C. 1996. Variations in the along-axis segmentation of the Afar Rift system.
903 *Tectonics*, **15**, 244-257.

904
905 Heine, C. & Müller, R. 2005. Late Jurassic rifting along the Australian North West Shelf: margin
906 geometry and spreading ridge configuration. *Australian Journal of Earth Sciences*, **52**, 27-39.

907
908 Hey, R. 1977. A new class of "pseudofaults" and their bearing on plate tectonics: A propagating rift
909 model. *Earth and Planetary Science Letters*, **37**, 321-325.

910
911 Hinz, K. 1981. A hypothesis on terrestrial catastrophies Wedges of very thick oceanward dipping
912 layers beneath passive continental margins. Their origin and paleoenvironmental significance.
913 *Geologisches Jahrbuch. Reihe E, Geophysik*, 3-28.

914
915 Hofmann, A. 2014. Sampling mantle heterogeneity through oceanic basalts: Isotopes and trace
916 elements. *In*: RW, C. (ed) *The Mantle and Core, Treatise on Geochemistry*. Elsevier-Pergamon,
917 Oxford, 67-101.

918
919 Holbourn, A.E. & Kaminski, M.A. 1995. Lower Cretaceous benthic foraminifera from DSDP Site 263:
920 micropalaeontological constraints for the early evolution of the Indian Ocean. *Marine*
921 *Micropaleontology*, **26**, 425-460.

922
923 Holford, S.P., Schofield, N., Jackson, C.A.L., Magee, C., Green, P.F. & Duddy, I.R. 2013. Impacts of
924 igneous intrusions on source and reservoir potential in prospective sedimentary basins along the
925 western Australian continental margin. *In*: Keep, M. & Moss, S.J. (eds) *The Sedimentary Basins of*
926 *Western Australia IV*. Proceedings of the Petroleum Exploration Society of Australia Symposium,
927 Perth, WA.

928
929 Hopper, J.R., Mutter, J.C., Larson, R.L. & Mutter, C.Z. 1992. Magmatism and rift margin evolution:
930 Evidence from northwest Australia. *Geology*, **20**, 853-857.

931
932 Karson, J.A. 2019. From Ophiolites to Oceanic Crust: Sheeted Dike Complexes and Seafloor
933 Spreading. *In*: Srivastava, R., Ernst, R. & Peng, P. (eds) *Dyke Swarms of the World: A Modern*
934 *Perspective*. Springer, 459-492.

935

936 Keranen, K., Klemperer, S., Gloaguen, R. & Group, E.W. 2004. Three-dimensional seismic imaging of a
937 protoridge axis in the Main Ethiopian rift. *Geology*, **32**, 949-952.

938
939 Larsen, H. & Saunders, A. 1998. 41. Tectonism and volcanism at the Southeast Greenland rifted
940 margin: a record of plume impact and later continental rupture. *Proceedings of the Ocean Drilling*
941 *Program, Scientific Results*, 503-533.

942
943 Larsen, H., Saunders, A. & Clift, P. 1994a. Proceedings of the Ocean Drilling Program, Initial Reports.
944 *Ocean Drilling Program*, College Station, Texas, 1-152.

945
946 Larsen, H., Saunders, A., Larsen, L. & Lykke-Andersen, H. 1994b. ODP activities on the South-East
947 Greenland margin: Leg 152 drilling and continued site surveying. *Rapport Grønlands Geologiske*
948 *Undersøgelse*, **160**, 75-81.

949
950 Larson, R.L., Mutter, J.C., Diebold, J.B., Carpenter, G.B. & Symonds, P. 1979. Cuvier Basin: a product
951 of ocean crust formation by Early Cretaceous rifting off Western Australia. *Earth and Planetary*
952 *Science Letters*, **45**, 105-114.

953
954 Lenoir, X., Féraud, G. & Geoffroy, L. 2003. High-rate flexure of the East Greenland volcanic margin:
955 constraints from 40Ar/39Ar dating of basaltic dykes. *Earth and Planetary Science Letters*, **214**, 515-
956 528.

957
958 Longley, I., Buessenschuett, C., Clydsdale, L., Cubitt, C., Davis, R., Johnson, M., Marshall, N., Murray,
959 A.*, et al.* 2002. The North West Shelf of Australia–a Woodside perspective. *The sedimentary basins of*
960 *Western Australia*, **3**, 27-88.

961
962 Mackenzie, G., Thybo, H. & Maguire, P. 2005. Crustal velocity structure across the Main Ethiopian
963 Rift: results from two-dimensional wide-angle seismic modelling. *Geophysical Journal International*,
964 **162**, 994-1006.

965
966 MacLeod, S.J., Williams, S.E., Matthews, K.J., Müller, R.D. & Qin, X. 2017. A global review and digital
967 database of large-scale extinct spreading centers. *Geosphere*, **13**, 911-949.

968
969 Maus, S., Barckhausen, U., Berkenbosch, H., Bournas, N., Brozena, J., Childers, V., Dostaler, F.,
970 Fairhead, J.*, et al.* 2009. EMAG2: A 2–arc min resolution Earth Magnetic Anomaly Grid compiled from
971 satellite, airborne, and marine magnetic measurements. *Geochemistry, Geophysics, Geosystems*, **10**.

972
973 McDermott, C., Lonergan, L., Collier, J.S., McDermott, K.G. & Bellingham, P. 2018. Characterization of
974 Seaward-Dipping Reflectors Along the South American Atlantic Margin and Implications for
975 Continental Breakup. *Tectonics*, **37**, 3303-3327.

976
977 McDermott, C., Collier, J.S., Lonergan, L., Fruehn, J. & Bellingham, P. 2019. Seismic velocity structure
978 of seaward-dipping reflectors on the South American continental margin. *Earth and Planetary*
979 *Science Letters*, **521**, 14-24.

Menard, H. 1969. Elevation and subsidence of oceanic crust. *Earth and Planetary Science Letters*, **6**, 275-284.

Menzies, M., Klemperer, S., Ebinger, C. & Baker, J. 2002. Characteristics of volcanic rifted margins. *In*: Menzies, M., Klemperer, S., Ebinger, C. & Baker, J. (eds) *Volcanic Rifted Margins, Special Publications*. Geological Society of America, **362**, 1-14.

Meyer, B., Chulliat, A. & Saltus, R. 2017. Derivation and error analysis of the Earth Magnetic Anomaly Grid at 2 arc min Resolution Version 3 (EMAG2v3). *Geochemistry, Geophysics, Geosystems*, **18**, 4522-4537.

Mihut, D. & Müller, R.D. 1998. Volcanic margin formation and Mesozoic rift propagators in the Cuvier Abyssal Plain off Western Australia. *Journal of Geophysical Research*, **103**, 27135-27127,27149.

Moulin, M., Aslanian, D. & Unternehr, P. 2010. A new starting point for the South and Equatorial Atlantic Ocean. *Earth-Science Reviews*, **98**, 1-37.

Mutter, J.C., Talwani, M. & Stoffa, P.L. 1982. Origin of seaward-dipping reflectors in oceanic crust off the Norwegian margin by "subaerial sea-floor spreading". *Geology*, **10**, 353-357.

Norcliffe, J.R., Paton, D.A., Mortimer, E.J., McCaig, A.M., Nicholls, H., Rodriguez, K., Hodgson, N. & Van Der Spuy, D. 2018. Laterally Confined Volcanic Successions (LCVS); recording rift-jumps during the formation of magma-rich margins. *Earth and Planetary Science Letters*, **504**, 53-63.

Olierook, H.K., Merle, R.E., Jourdan, F., Sircombe, K., Fraser, G., Timms, N.E., Nelson, G., Dadd, K.A*., et al.* 2015. Age and geochemistry of magmatism on the oceanic Wallaby Plateau and implications for the opening of the Indian Ocean. *Geology*, **43**, 971-974.

Oosting, A., Leereveld, H., Dickens, G., Henderson, R. & Brinkhuis, H. 2006. Correlation of Barremian-Aptian (mid-Cretaceous) dinoflagellate cyst assemblages between the Tethyan and Austral realms. *Cretaceous Research*, **27**, 792-813.

Parsons, B. & Sclater, J.G. 1977. An analysis of the variation of ocean floor bathymetry and heat flow with age. *Journal of Geophysical Research*, **82**, 803-827.

Paton, D., Pindell, J., McDermott, K., Bellingham, P. & Horn, B. 2017. Evolution of seaward-dipping reflectors at the onset of oceanic crust formation at volcanic passive margins: Insights from the South Atlantic. *Geology*, **45**, 439-442.

Phipps-Morgan, J. & Chen, Y.J. 1993. The genesis of oceanic crust: Magma injection, hydrothermal circulation, and crustal flow. *Journal of Geophysical Research: Solid Earth*, **98**, 6283-6297.

1024 Plank, T. & Langmuir, C.H. 1998. The chemical composition of subducting sediment and its
1025 consequences for the crust and mantle. *Chemical Geology*, **145**, 325-394.

1026
1027 Planke, S. & Eldholm, O. 1994. Seismic response and construction of seaward dipping wedges of
1028 flood basalts: Vøring volcanic margin. *Journal of Geophysical Research: Solid Earth*, **99**, 9263-9278.

1029
1030 Planke, S., Symonds, P.A., Alvestad, E. & Skogseid, J. 2000. Seismic volcanostratigraphy of large-
1031 volume basaltic extrusive complexes on rifted margins. *Journal of Geophysical Research: Solid Earth*,
1032 **105**, 19335-19351.

1033
1034 Rabinowitz, P.D. & LaBrecque, J. 1979. The Mesozoic South Atlantic Ocean and evolution of its
1035 continental margins. *Journal of Geophysical Research: Solid Earth*, **84**, 5973-6002.

1036
1037 Rey, S.S., Planke, S., Symonds, P.A. & Faleide, J.I. 2008. Seismic volcanostratigraphy of the Gascoyne
1038 margin, Western Australia. *Journal of Volcanology and Geothermal Research*, **172**, 112-131,
1039 http://doi.org/10.1016/j.jvolgeores.2006.11.013.

1040
1041 Robb, M.S., Taylor, B. & Goodliffe, A.M. 2005. Re-examination of the magnetic lineations of the
1042 Gascoyne and Cuvier Abyssal Plains, off NW Australia. *Geophysical Journal International*, **163**, 42-55.

1043
1044 Roberts, D., Backman, J., Morton, A., Murray, J. & Keene, J. 1984. *Evolution of volcanic rifted margins*
1045 *– synthesis of leg-81 results on the West margin of Rockall Plateau*.

1046
1047 Robinson, P.T., Thayer, P., Cook, P., McKnight, B. & et al. 1974. *Lithology of Mesozoic and Cenozoic*
1048 *sediments of the eastern Indian Ocean, Leg 27, Deep Sea Drilling Project*.

1049
1050 Rudnick, R.L. & Fountain, D.M. 1995. Nature and composition of the continental crust: a lower
1051 crustal perspective. *Reviews of Geophysics*, **33**, 267-309.

1052
1053 Sayers, J., Borissova, I., Ramsay, D. & Symonds, P. 2002. *Geological framework of the Wallaby*
1054 *Plateau and adjacent areas*.

1055
1056 Scheibnerová, V. 1974. *Aptian–Albian benthonic foraminifera from DSDP Leg 27, Sites 259, 260 and*
1057 *263, Eastern Indian Ocean*.

1058
1059 Skogseid, J., Pedersen, T., Eldholm, O. & Larsen, B.T. 1992. Tectonism and magmatism during NE
1060 Atlantic continental break-up: the Voring Margin. *Geological Society, London, Special Publications*,
1061 **68**, 305-320, http://doi.org/10.1144/gsl.sp.1992.068.01.19.

1062
1063 Skogseid, J., Planke, S., Faleide, J.I., Pedersen, T., Eldholm, O. & Neverdal, F. 2000. NE Atlantic
1064 continental rifting and volcanic margin formation. *In*: Nottvedt, A. (ed) *Dynamics of the Norwegian*
1065 *Margin*. Geological Society, London, Special Publications, London, **167**, 295-326.

1066

Stagg, H., Alcock, M., Bernardel, G., Moore, A., Symonds, P. & Exon, N. 2004. *Geological framework of the outer Exmouth Plateau and adjacent ocean basins*. Geoscience Australia.

Stein, C.A. & Stein, S. 1992. A model for the global variation in oceanic depth and heat flow with lithospheric age. *Nature*, **359**, 123.

Stilwell, J., Quilty, P. & Mantle, D. 2012. Paleontology of Early Cretaceous deep-water samples dredged from the Wallaby Plateau: new perspectives of Gondwana break-up along the Western Australian margin. *Australian Journal of Earth Sciences*, **59**, 29-49.

Sun, S.-S. & McDonough, W.F. 1989. Chemical and isotopic systematics of oceanic basalts: implications for mantle composition and processes. *In*: Saunders, A. & Norry, M. (eds) *Magmatism in Ocean Basins*. Geological Society, London, Special Publications, **42**, 313-345.

Symonds, P.A., Planke, S., Frey, O. & Skogseid, J. 1998. Volcanic evolution of the Western Australian Continental Margin and its implications for basin development. *The Sedimentary Basins of Western Australia 2: Proc. of Petroleum Society Australia Symposium, Perth, WA*.

Talwani, M. & Eldholm, O. 1973. Boundary between continental and oceanic crust at the margin of rifted continents. *Nature*, **241**, 325.

Tian, X. & Buck, W.R. 2019. Lithospheric thickness of volcanic rifting margins: Constraints from seaward dipping reflectors. *Journal of Geophysical Research: Solid Earth*, **124**, 3254-3270.

Tischer, M. 2006. *The structure and development of the continent-ocean transition zone of the Exmouth Plateau and Cuvier margin, Northwest Australia: implications for extensional strain partitioning.* PhD, Columbia University.

Tivey, M.A., Johnson, H.P., Fleutelot, C., Hussenoeder, S., Lawrence, R., Waters, C. & Wooding, B. 1998. Direct measurement of magnetic reversal polarity boundaries in a cross-section of oceanic crust. *Geophysical Research Letters*, **25**, 3631-3634.

Veevers, J. 1986. Breakup of Australia and Antarctica estimated as mid-Cretaceous (95±5 Ma) from magnetic and seismic data at the continental margin. *Earth and Planetary Science Letters*, **77**, 91-99.

Veevers, J. & Johnstone, M. 1974. Comparative stratigraphy and structure of the western Australian margin and the adjacent deep ocean floor. *Initial Reports of the Deep Sea Drilling Project*, **27**, 571-585.

Vine, F.J. 1966. Spreading of the ocean floor: new evidence. *Science*, **154**, 1405-1415, http://doi.org/10.1126/science.154.3755.1405.

Vine, F.J. & Matthews, D.H. 1963. Magnetic anomalies over oceanic ridges. *Nature*, **199**, 947-949.

Wiseman, J.F. & Williams, A. 1974. *Palynological investigation of samples from sites 259, 261, and 263, Leg 27, Deep Sea Drilling Project*.

Table 1: Average interval velocities obtained from OBS array

| Layer | Seismic velocity (km $s^{-1}$) |
|---|---|
| Water column | 1.5 |
| Sedimentary strata | 2.0–2.8 |
| Seaward-dipping reflectors (SDRs) | 4.9 |
| Sub-SDR crust | 6.8–7.2 |
| Upper mantle | 8 |

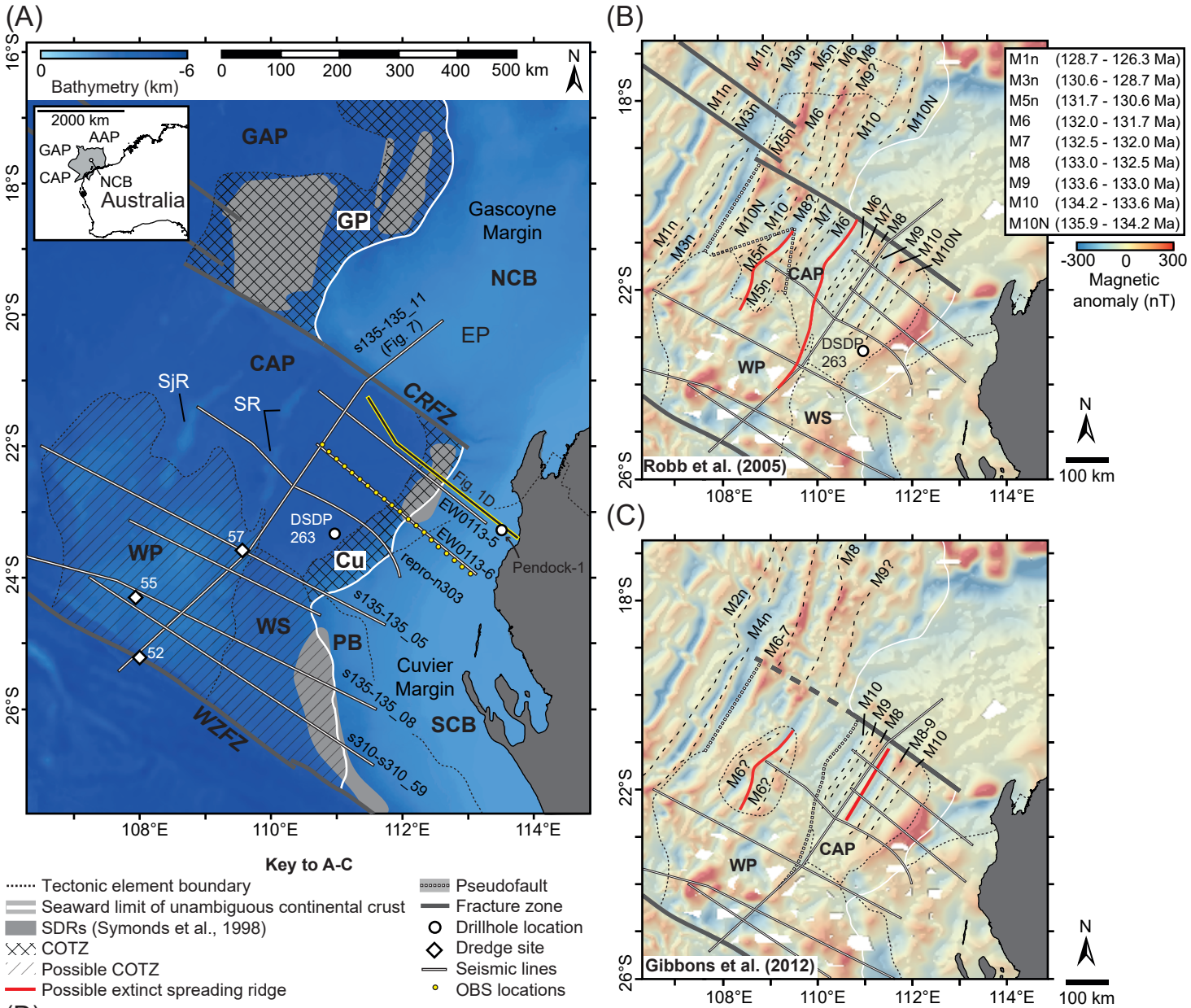
(A)
Bathymetry (km)
0
-6
0
100
200
300
400
500 km
N
2000 km
AAP
GAP
CAP
NCB
Australia
GAP
GP
Gascoyne Margin
NCB
EP
CAP
SjR
SR
CRFZ
s135-135_11 (Fig. 7)
Fig. 1D
EW0113-5
EW0113-6
repro-n303
DSDP 263
Cu
Pendock-1
WP
57
55
52
WS
PB
Cuvier Margin
SCB
WZFZ
s135-135_05
s135-135_08
s310-s310_59
16°S
18°S
20°S
22°S
24°S
26°S
108°E
110°E
112°E
114°E
(B)
M1n (128.7 - 126.3 Ma)
M3n (130.6 - 128.7 Ma)
M5n (131.7 - 130.6 Ma)
M6 (132.0 - 131.7 Ma)
M7 (132.5 - 132.0 Ma)
M8 (133.0 - 132.5 Ma)
M9 (133.6 - 133.0 Ma)
M10 (134.2 - 133.6 Ma)
M10N (135.9 - 134.2 Ma)
-300
0
300
Magnetic anomaly (nT)
CAP
WP
WS
DSDP 263
Robb et al. (2005)
N
100 km
(C)
M2n
M4n
M6-7
M8
M9?
M10
M9
M8
M8-9
M10
M6?
M6?
CAP
WP
Gibbons et al. (2012)
N
100 km
Key to A-C
Tectonic element boundary
Seaward limit of unambiguous continental crust
SDRs (Symonds et al., 1998)
COTZ
Possible COTZ
Possible extinct spreading ridge
Pseudofault
Fracture zone
Drillhole location
Dredge site
Seismic lines
OBS locations

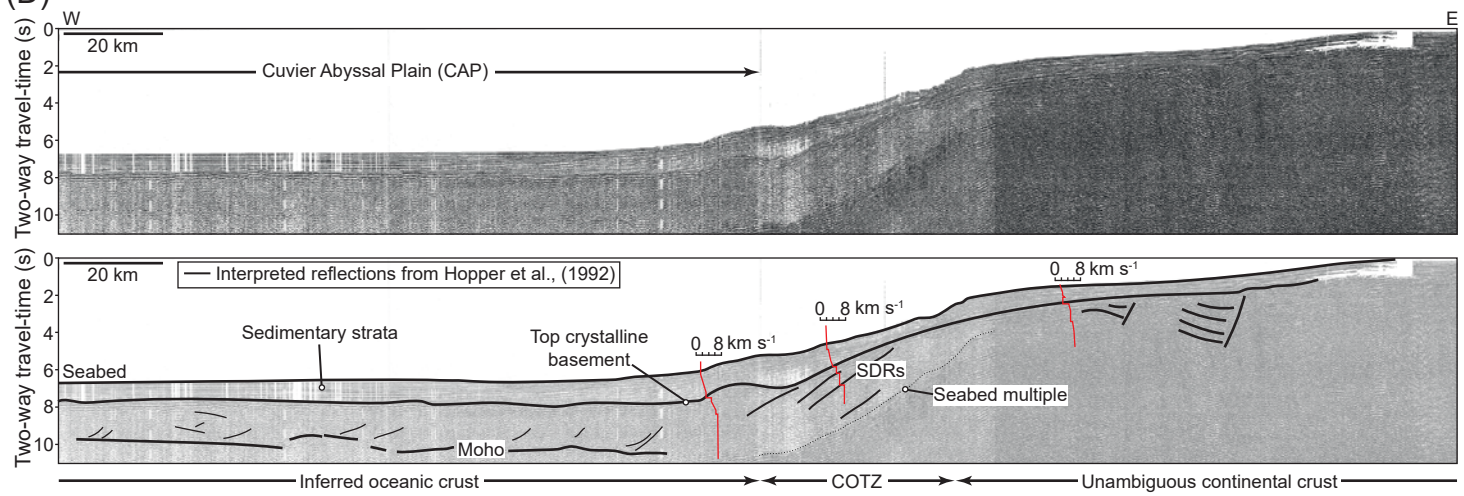
(D)
W
E
20 km
Cuvier Abyssal Plain (CAP)
Two-way travel-time (s)
20 km
Interpreted reflections from Hopper et al., (1992)
Sedimentary strata
Top crystalline basement
Seabed
Moho
SDRs
Seabed multiple
0 8 km s-1
Inferred oceanic crust
COTZ
Unambiguous continental crust

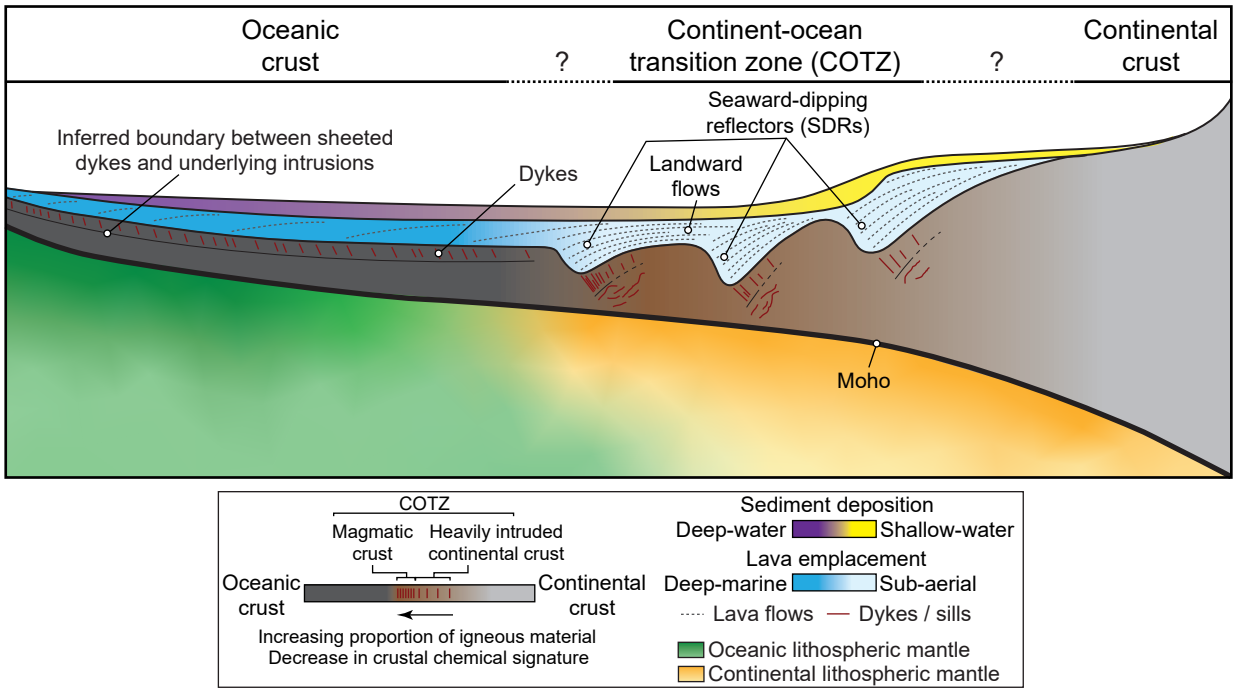
Oceanic crust
?
Continent-ocean transition zone (COTZ)
?
Continental crust
Inferred boundary between sheeted dykes and underlying intrusions
Dykes
Seaward-dipping reflectors (SDRs)
Landward flows
Moho


COTZ
Magmatic crust
Heavily intruded continental crust
Oceanic crust
Continental crust
Increasing proportion of igneous material
Decrease in crustal chemical signature
Sediment deposition
Deep-water
Shallow-water
Lava emplacement
Deep-marine
Sub-aerial
Lava flows
Dykes / sills
Oceanic lithospheric mantle
Continental lithospheric mantle

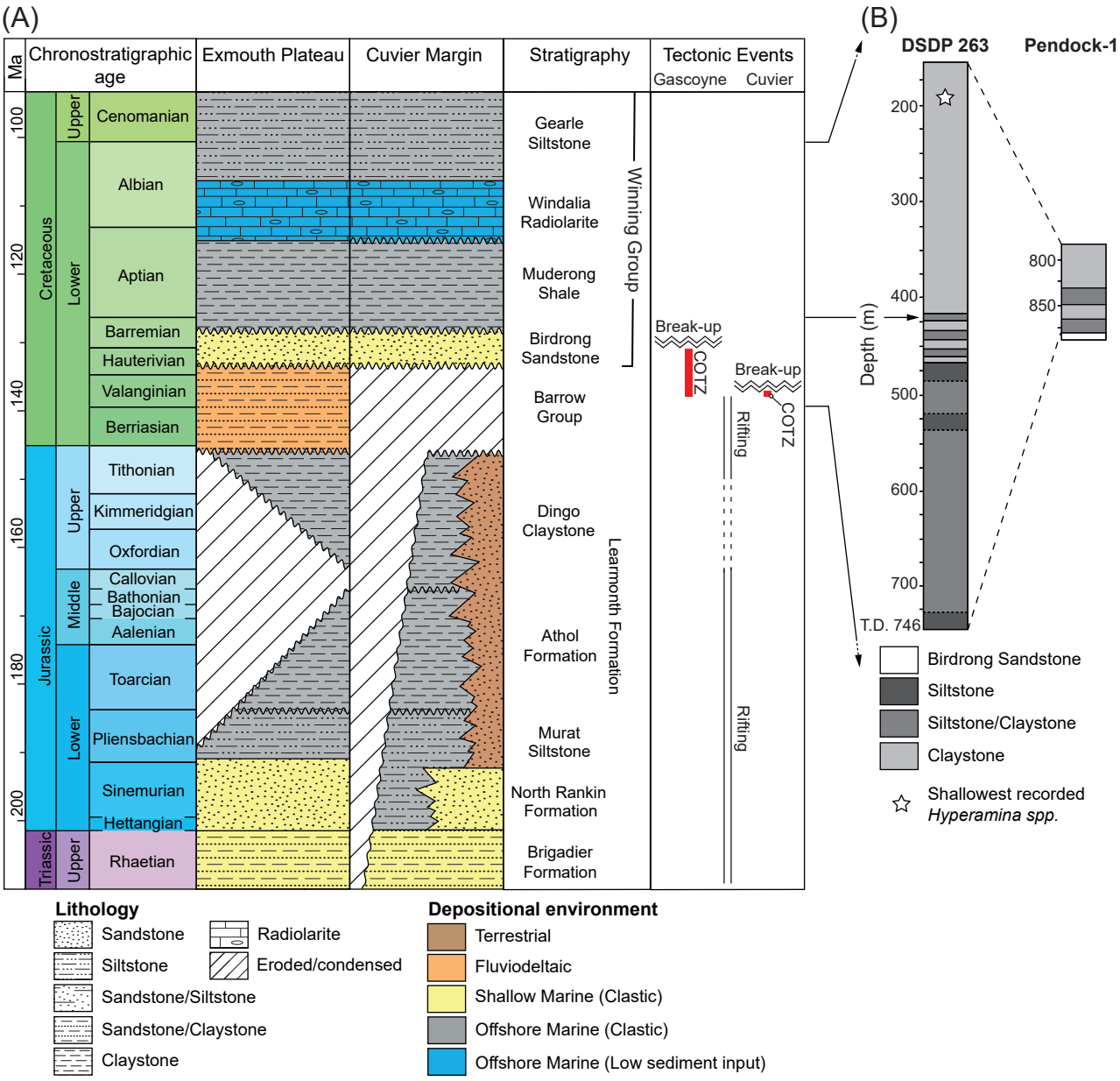
(A)
Ma
Chronostratigraphic age
Exmouth Plateau
Cuvier Margin
Stratigraphy
Tectonic Events
Gascoyne
Cuvier
Cretaceous
Upper
Lower
Jurassic
Middle
Upper
Lower
Triassic
Upper
Cenomanian
Albian
Aptian
Barremian
Hauterivian
Valanginian
Berriasian
Tithonian
Kimmeridgian
Oxfordian
Callovian
Bathonian
Bajocian
Aalenian
Toarcian
Pliensbachian
Sinemurian
Hettangian
Rhaetian
100
120
140
160
180
200
Gearle Siltstone
Windalia Radiolarite
Muderong Shale
Birdrong Sandstone
Barrow Group
Dingo Claystone
Athol Formation
Murat Siltstone
North Rankin Formation
Brigadier Formation
Winning Group
Learmonth Formation
Break-up
COTZ
Break-up
COTZ
Rifting
Rifting
(B)
DSDP 263
Pendock-1
Depth (m)
200
300
400
500
600
700
800
850
T.D. 746
Birdrong Sandstone
Siltstone
Siltstone/Claystone
Claystone
Shallowest recorded
Hyperamina spp.
Lithology
Sandstone
Siltstone
Sandstone/Siltstone
Sandstone/Claystone
Claystone
Radiolarite
Eroded/condensed
Depositional environment
Terrestrial
Fluviodeltaic
Shallow Marine (Clastic)
Offshore Marine (Clastic)
Offshore Marine (Low sediment input)

Figure 4

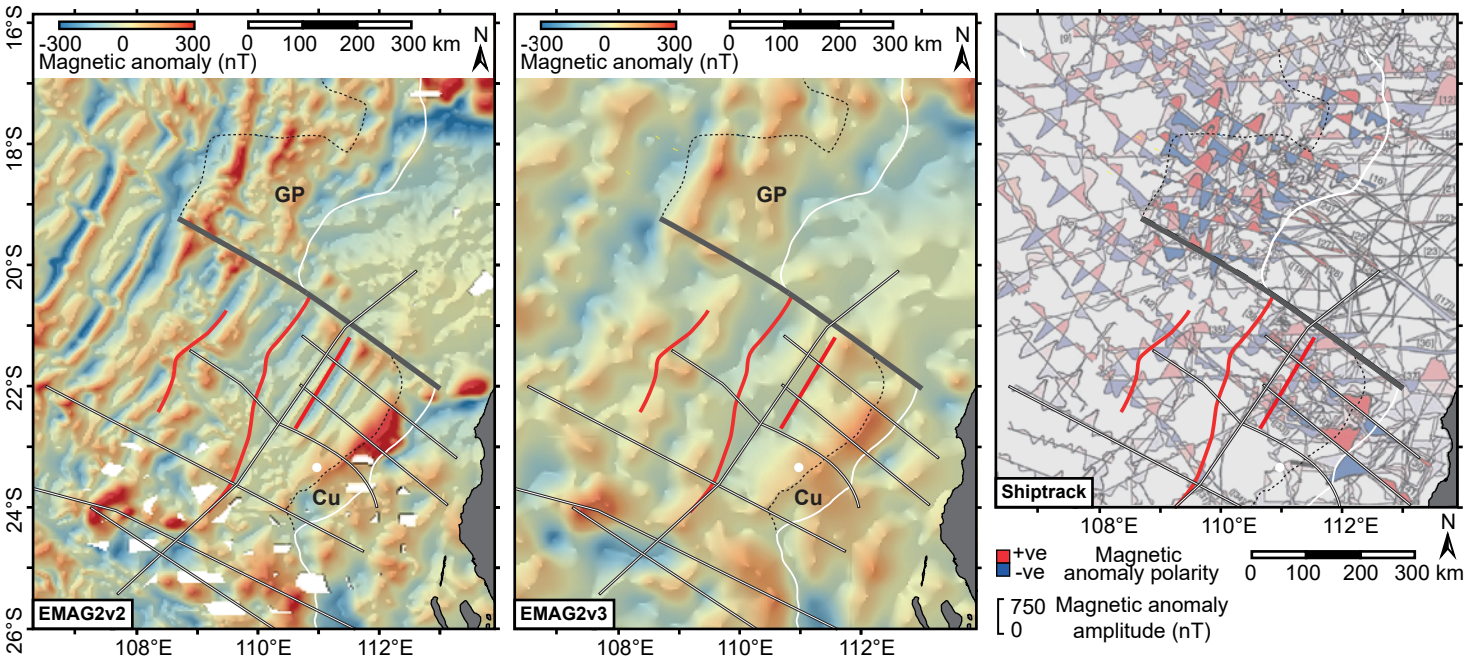
-300 0 300
Magnetic anomaly (nT)
0 100 200 300 km
N
GP
Cu
EMAG2v2
EMAG2v3
Shiptrack
16°S
18°S
20°S
22°S
24°S
26°S
108°E
110°E
112°E
+ve
-ve
Magnetic anomaly polarity
750
0
Magnetic anomaly amplitude (nT)

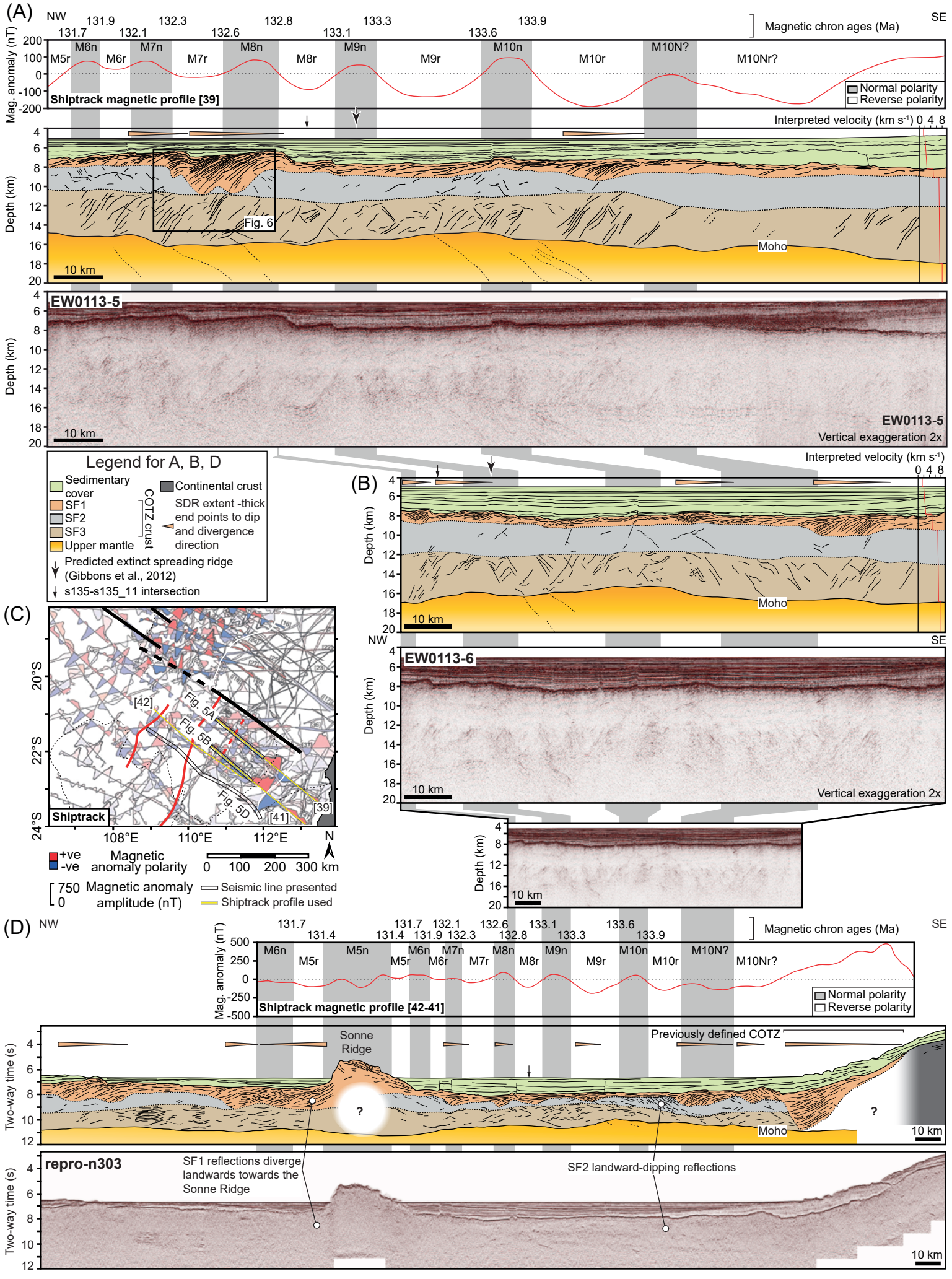
(A)
NW
SE
Magnetic chron ages (Ma)
Mag. anomaly (nT)
Shiptrack magnetic profile [39]
Normal polarity
Reverse polarity
Interpreted velocity (km s-1)
Depth (km)
Fig. 6
Moho
10 km
EW0113-5
Vertical exaggeration 2x
Legend for A, B, D
Sedimentary cover
SF1
SF2
SF3
Upper mantle
COTZ crust
Continental crust
SDR extent -thick end points to dip and divergence direction
Predicted extinct spreading ridge (Gibbons et al., 2012)
s135-s135_11 intersection
(B)
EW0113-6
(C)
Shiptrack
Fig. 5A
Fig. 5B
Fig. 5D
[42]
[39]
[41]
20°S
22°S
24°S
108°E
110°E
112°E
N
+ve
-ve
Magnetic anomaly polarity
0 100 200 300 km
750
0
Magnetic anomaly amplitude (nT)
Seismic line presented
Shiptrack profile used
(D)
Shiptrack magnetic profile [42-41]
Previously defined COTZ
Sonne Ridge
Two-way time (s)
repro-n303
SF1 reflections diverge landwards towards the Sonne Ridge
SF2 landward-dipping reflections

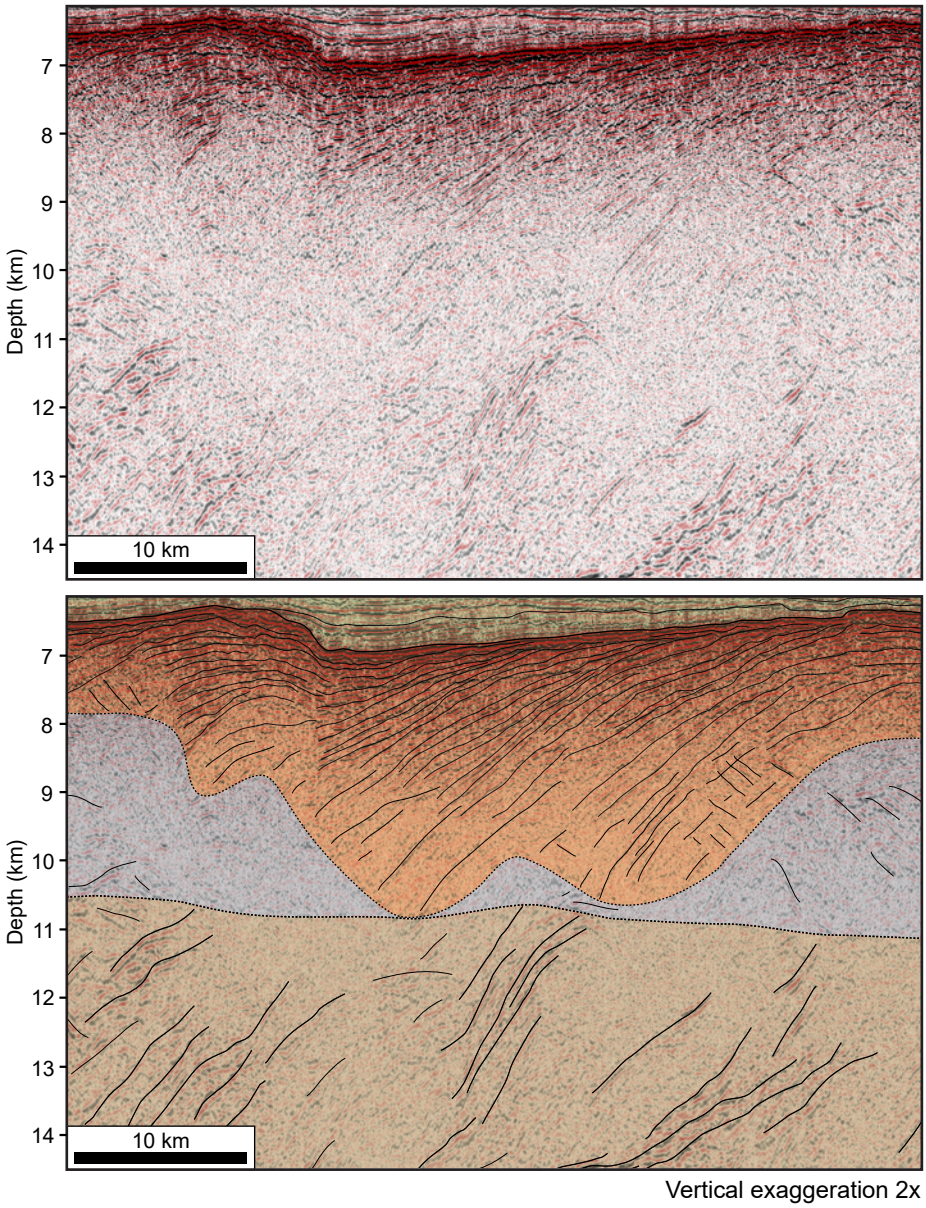
Depth (km)
7
8
9
10
11
12
13
14
10 km
Depth (km)
7
8
9
10
11
12
13
14
10 km
Vertical exaggeration 2x

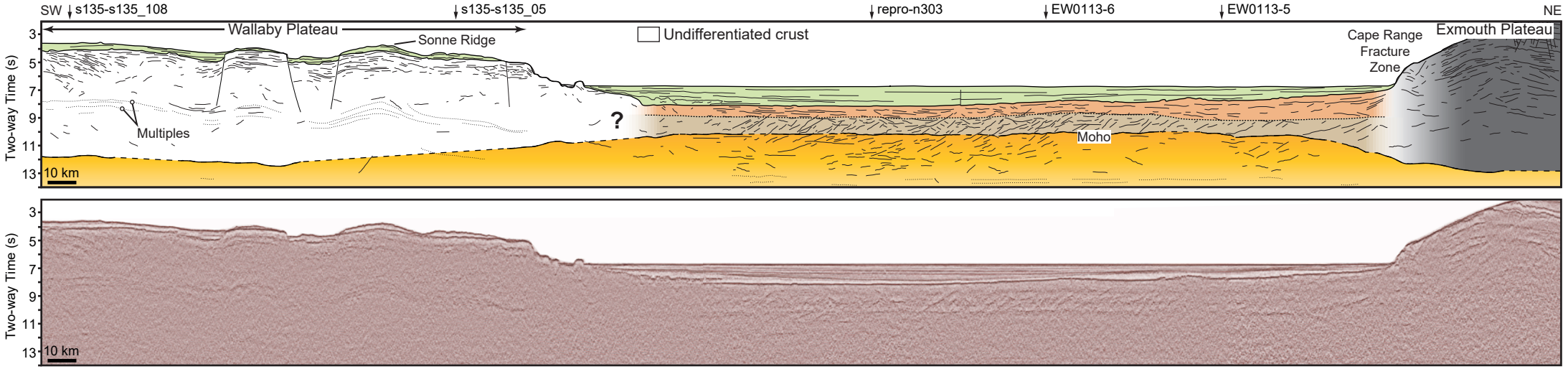
SW
s135-s135_108
s135-s135_05
repro-n303
EW0113-6
EW0113-5
NE
Wallaby Plateau
Sonne Ridge
Undifferentiated crust
Cape Range
Fracture
Zone
Exmouth Plateau
Multiples
?
Moho
Two-way Time (s)
3
5
7
9
11
13
10 km

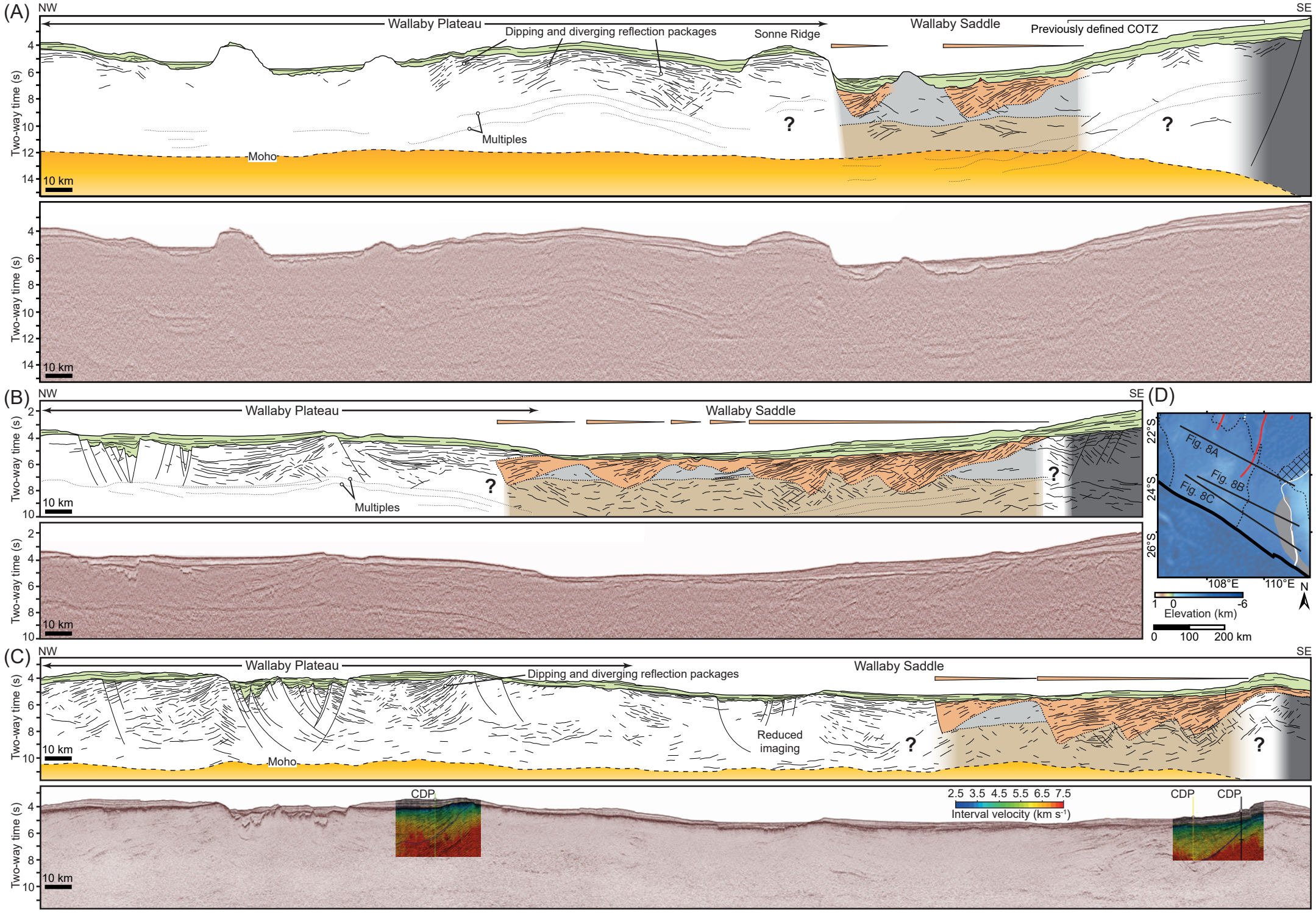
(A)
NW
SE
Wallaby Plateau
Dipping and diverging reflection packages
Sonne Ridge
Wallaby Saddle
Previously defined COTZ
Multiples
Moho
10 km
Two-way time (s)
(B)
Wallaby Plateau
Wallaby Saddle
Multiples
(C)
Wallaby Plateau
Dipping and diverging reflection packages
Wallaby Saddle
Reduced imaging
Moho
CDP
2.5 3.5 4.5 5.5 6.5 7.5
Interval velocity (km s⁻¹)
(D)
Fig. 8A
Fig. 8B
Fig. 8C
22°S
24°S
26°S
108°E
110°E
N
1 0 -6
Elevation (km)
0 100 200 km

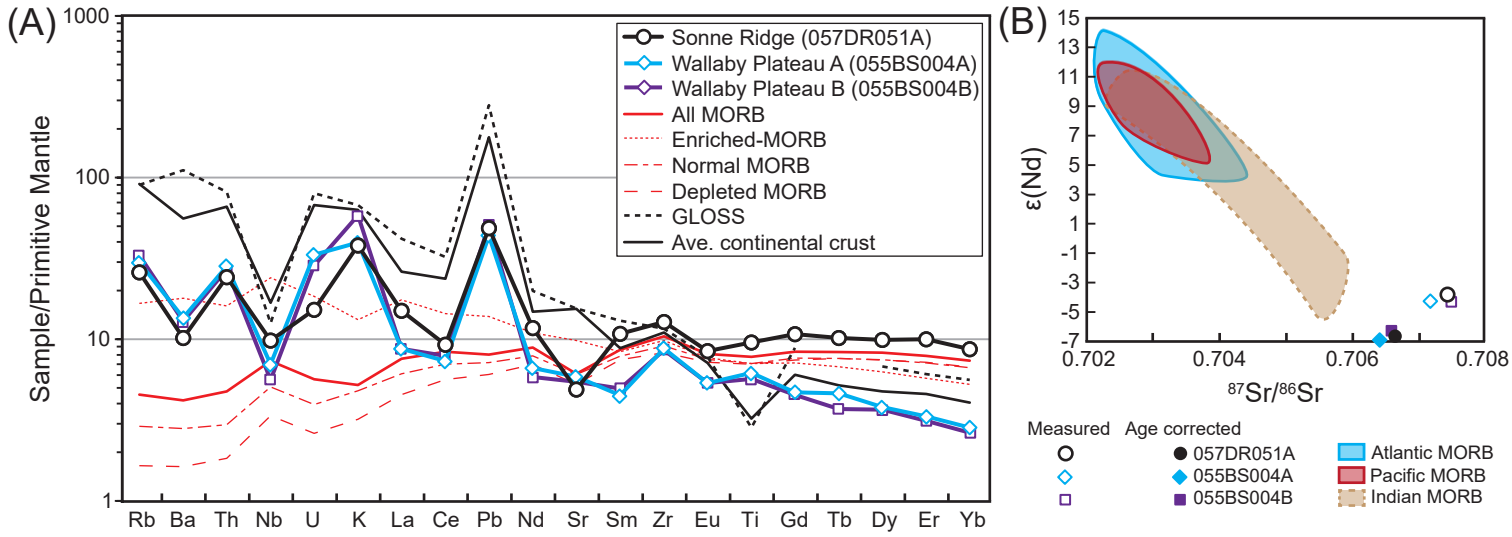
(A)
Sample/Primitive Mantle
1000
100
10
1
Rb Ba Th Nb U K La Ce Pb Nd Sr Sm Zr Eu Ti Gd Tb Dy Er Yb
Sonne Ridge (057DR051A)
Wallaby Plateau A (055BS004A)
Wallaby Plateau B (055BS004B)
All MORB
Enriched-MORB
Normal MORB
Depleted MORB
GLOSS
Ave. continental crust
(B)
ε(Nd)
15
13
11
9
7
5
3
1
-1
-3
-5
-7
0.702
0.704
0.706
0.708
87Sr/86Sr
Measured
Age corrected
057DR051A
055BS004A
055BS004B
Atlantic MORB
Pacific MORB
Indian MORB

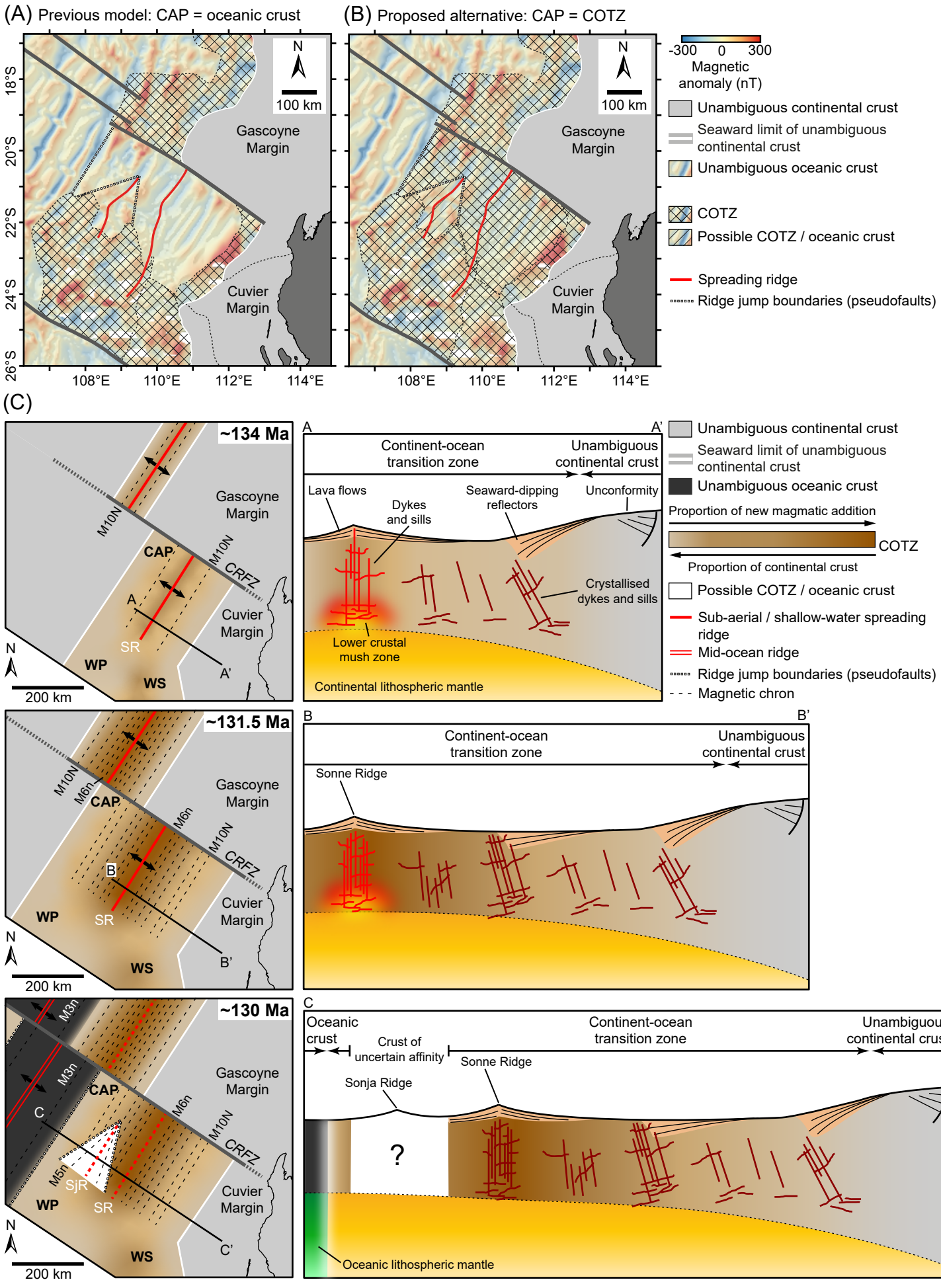
(A) Previous model: CAP = oceanic crust
(B) Proposed alternative: CAP = COTZ
18°S
20°S
22°S
24°S
26°S
108°E
110°E
112°E
114°E
N
100 km
Gascoyne Margin
Cuvier Margin
-300 0 300
Magnetic anomaly (nT)
Unambiguous continental crust
Seaward limit of unambiguous continental crust
Unambiguous oceanic crust
COTZ
Possible COTZ / oceanic crust
Spreading ridge
Ridge jump boundaries (pseudofaults)
(C)
~134 Ma
~131.5 Ma
~130 Ma
M10N
M6n
M3n
M5n
CAP
CRFZ
SjR
SR
WP
WS
A
A'
B
B'
C
C'
200 km
Continent-ocean transition zone
Unambiguous continental crust
Lava flows
Dykes and sills
Seaward-dipping reflectors
Unconformity
Crystallised dykes and sills
Lower crustal mush zone
Continental lithospheric mantle
Proportion of new magmatic addition
Proportion of continental crust
Possible COTZ / oceanic crust
Sub-aerial / shallow-water spreading ridge
Mid-ocean ridge
Ridge jump boundaries (pseudofaults)
Magnetic chron
Sonne Ridge
Oceanic crust
Crust of uncertain affinity
Sonja Ridge
?
Oceanic lithospheric mantle